Article

SOURCE DATA | TRANSPARENT PROCESS | OPEN ACCESS | CHECK FOR UPDATES

EMBO reports

BRD4 isoforms have distinct roles in tumour progression and metastasis in rhabdomyosarcoma

Dipanwita Das[1], Jia Yu Leung[1,2,3], Shivaranjani Balamurugan[1], Vinay Tergaonkar[2,3,4], Amos Hong Pheng Loh[5], Cheng-Ming Chiang[6,7,8] & Reshma Taneja[1]✉

Abstract

BRD4, a bromodomain and extraterminal (BET) protein, is deregulated in multiple cancers and has emerged as a promising drug target. However, the function of the two main BRD4 isoforms (BRD4-L and BRD4-S) has not been analysed in parallel in most cancers. This complicates determining therapeutic efficacy of pan-BET inhibitors. In this study, using functional and transcriptomic analysis, we show that BRD-L and BRD4-S isoforms play distinct roles in fusion negative embryonal rhabdomyosarcoma. BRD4-L has an oncogenic role and inhibits myogenic differentiation, at least in part, by activating myostatin expression. Depletion of BRD4-L in vivo impairs tumour progression but does not impact metastasis. On the other hand, depletion of BRD4-S has no significant impact on tumour growth, but strikingly promotes metastasis in vivo. Interestingly, BRD4-S loss results in the enrichment of BRD4-L and RNA Polymerase II at integrin gene promoters resulting in their activation. In fusion positive alveolar rhabdomyosarcoma, BRD4-L is unrestricted in its oncogenic role, with no evident involvement of BRD4-S. Our work unveils isoform-specific functions of BRD4 in rhabdomyosarcoma.

Keywords Epigenetics; Metastasis; Differentiation; Myostatin; Integrins
Subject Categories Cancer; Chromatin, Transcription & Genomics; Signal Transduction
https://doi.org/10.1038/s44319-023-00033-1
Received 25 July 2023; Revised 27 November 2023; Accepted 5 December 2023
Published online: 8 January 2024

Introduction

Rhabdomyosarcoma (RMS), one of the most common soft tissue sarcomas among paediatric patients, arises due to a block in myogenic differentiation. RMS tumour cells fail to differentiate terminally despite expression of core myogenic transcription factors (Hawkins et al, 2013). RMS is traditionally classified into two major subtypes: alveolar (ARMS) and embryonal (ERMS), which account for 20% and 70% of RMS cases, respectively (Xia et al, 2002; Parham and Barr, 2013). PAX3-FOXO1 and PAX7-FOXO1 fusion proteins are present in about 70–80% of ARMS but absent in ERMS. ARMS with fusion positive (FP) status is associated with worse prognosis. Patients with fusion negative ARMS have clinical outcomes similar to ERMS (Williamson et al, 2010; Shern et al, 2014).

In ERMS, loss of heterozygosity on the short arm of chromosome 11(11p15.5) leads to inactivation of tumour suppressor genes (Loh et al, 1992). The overall survival rate for patients with relapsed or metastatic RMS remains as low as 21% and 30%, respectively. RMS is characterized by an aberrant epigenetic landscape. Altered expression of DNA methyltransferases and demethylases, microRNAs and enzymes involved in histone methylation, phosphorylation and acetylation has been observed. This leads to altered expression of genes involved in cellular proliferation, DNA replication, differentiation, epithelial-mesenchymal transition (EMT) and tumour progression. Epigenetic reprogramming thus provides an opportunity to identify novel druggable targets (Megiorni, 2020).

Bromodomain-containing protein 4 (BRD4), a member of bromodomain and extraterminal (BET) family, is an epigenetic regulator that plays an important role in embryogenesis and cancer development (Donati et al, 2018). The BET family proteins are acetyl-lysine readers, which primarily bind to acetylated chromatin and transcription factors (Wu and Chiang, 2007). The BET proteins are characterized by two tandem bromodomains (BD1 and BD2), which bind acetylated lysine residues on target proteins (Zeng and Zhou, 2002). BRD4, along with other BET proteins, accumulates on active transcription regulatory elements and enhances gene transcription in both the initiation and elongation phase (Chiang, 2009).

BRD4 gene encodes two major naturally occurring splice variants: BRD4-long (BRD4-L) and BRD4-short (BRD4-S) isoforms. The two variants are generated in a constant and balanced ratio to ensure homeostatic functioning of the protein (Wu et al, 2020). BRD4-L has an extended proline-rich region and a positive transcription elongation factor (P-TEFb)-interacting region at its C-terminal motif (CTM; see Fig. 1A), while BRD4-S with

[1]Department of Physiology, Healthy Longevity and NUS Center for Cancer Research Translation Research Programme, Yong Loo Lin School of Medicine, National University of Singapore, Singapore 117593, Singapore. [2]Institute of Molecular and Cell Biology (IMCB), Agency for Science, Technology and Research (A*STAR), Singapore 138673, Singapore. [3]Department of Pathology, Yong Loo Lin School of Medicine, National University of Singapore, Singapore 119074, Singapore. [4]Department of Biochemistry, Yong Loo Lin School of Medicine, National University of Singapore, Singapore 117596, Singapore. [5]VIVA-KKH Paediatric Brain and Solid Tumour Programme, KK Women's and Children's Hospital, Singapore 229899, Singapore. [6]Simmons Comprehensive Cancer Center, University of Texas Southwestern Medical Center, Dallas, TX 75390, USA. [7]Department of Biochemistry, University of Texas Southwestern Medical Center, Dallas, TX 75390, USA. [8]Department of Pharmacology, University of Texas Southwestern Medical Center, Dallas, TX 75390, USA. ✉E-mail: phsrt@nus.edu.sg

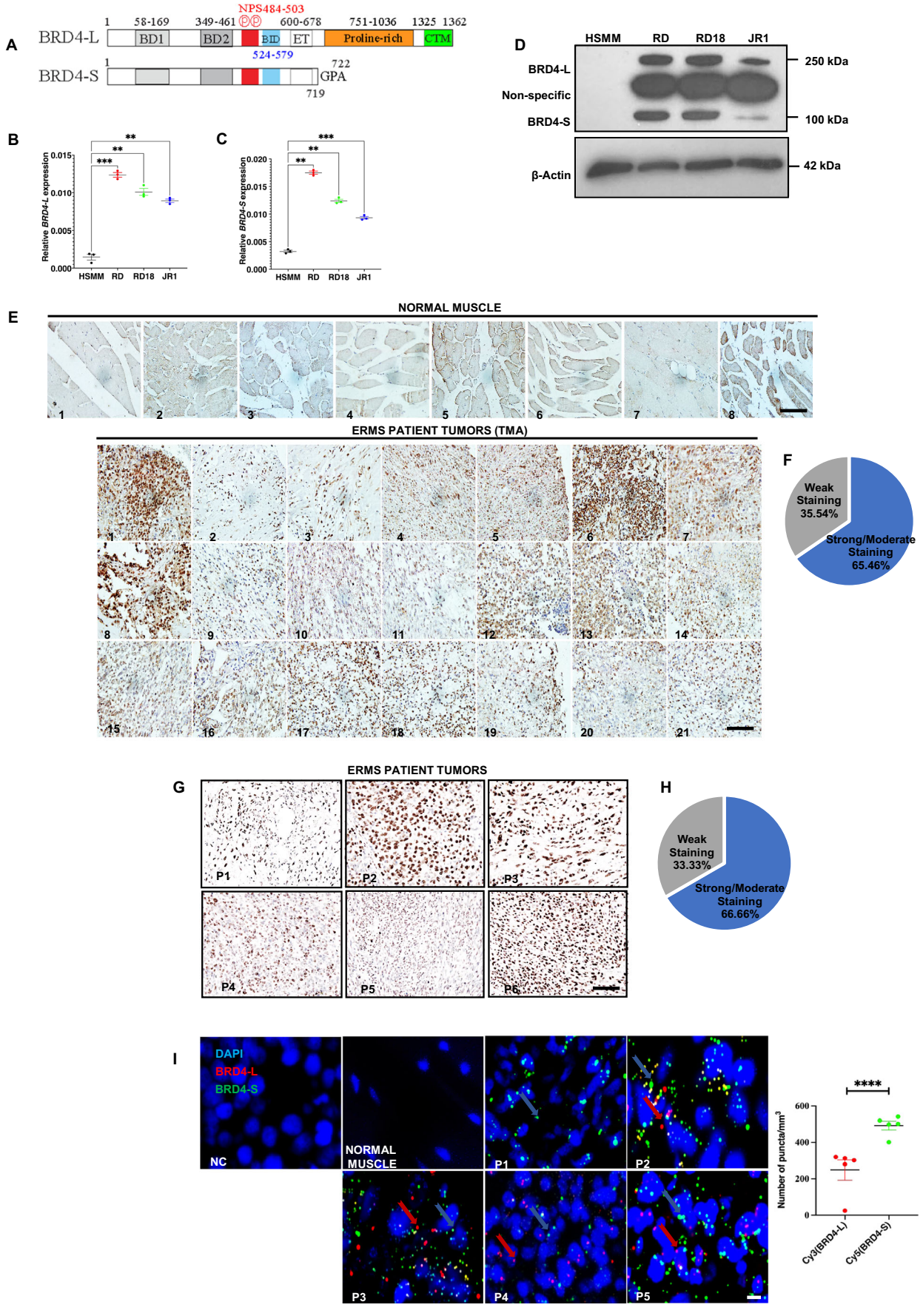
A
NPS484-503
1
58-169
349-461
600-678
751-1036
1325
1362
BRD4-L
BD1
BD2
BID
ET
Proline-rich
CTM
524-579
BRD4-S
722
GPA
719
B
Relative BRD4-L expression
HSMM
RD
RD18
JR1
C
Relative BRD4-S expression
D
HSMM
RD
RD18
JR1
BRD4-L
Non-specific
BRD4-S
β-Actin
250 kDa
100 kDa
42 kDa
E
NORMAL MUSCLE
ERMS PATIENT TUMORS (TMA)
F
Weak Staining 35.54%
Strong/Moderate Staining 65.46%
G
ERMS PATIENT TUMORS
P1
P2
P3
P4
P5
P6
H
Weak Staining 33.33%
Strong/Moderate Staining 66.66%
I
DAPI
BRD4-L
BRD4-S
NC
NORMAL MUSCLE
P1
P2
P3
P4
P5
Number of puncta/mm3
Cy3(BRD4-L)
Cy5(BRD4-S)
****

Figure 1. BRD4 is overexpressed in ERMS.

(A) Schematic presentation of BRD4-L and BRD4-S domain structure. **(B,C)** BRD4-L and BRD4-S mRNA levels were examined in HSMM, RD, RD18 and JR1 by RT-qPCR analysis. Values correspond to the average ± SEM ($n = 3$ biological replicates with average of 3 technical replicates shown). Statistical significance was calculated by one-way ANOVA analysis. $^{**}p \leq 0.01$, $^{***}p \leq 0.001$. **(D)** Western blot analysis showing expression of BRD4-L and BRD4-S isoforms in HSMM, RD, RD18 and JR1 cell lines. β-Actin was used as loading control. Images are representative of at least three biological replicates. **(E)** TMA consisting of 8 normal skeletal muscle samples and 21 ERMS patient tumours was analysed by IHC using anti-BRD4 antibody. Images were taken at ×40 magnification. Scale bar: 100 μm. **(F)** Pie chart illustrating the distribution of staining intensities in the TMA samples. **(G)** Six archival ERMS tumour specimens (P1–P6) were analysed by IHC using anti-BRD4 antibody. Images were taken at ×40 magnification. Scale bar: 100 μm. **(H)** Pie chart illustrating the distribution of staining intensities in ERMS patient samples. **(I)** Detection of BRD4-L and BRD4-S RNA transcripts in ERMS patient tumour specimens (P1–P5) using RNAscope assay. BRD4-L and BRD4-S transcripts were quantified as red and green puncta, respectively, and are presented as a scatter plot. A field with ~50 nuclei was chosen for quantification. No signal was observed in the negative control (NC) and normal skeletal muscle. At least 3 fields were imaged for each patient sample and one representative image is shown. Nuclei were stained with DAPI (blue). The signal for each isoform is shown by colour-coded arrows. Values correspond to the average ± SEM. Two-tailed non-parametric unpaired t test was performed for statistical analysis. $^{****}p \leq 0.0001$. Scale bar: 20 μm. Source data are available online for this figure.

phase-separation properties, functions to organize chromatin and transcription factors for activation of gene transcription (Han et al, 2020). BRD4-L and Mediator together form the transcription initiation complex, which along with P-TEFb then phosphorylates dual serine residues (Ser5 and Ser2) in RNA Polymerase (Pol) II and modulates transcription initiation and early elongation (Chiang, 2009; Devaiah et al, 2012). BRD4-S, on the other hand, contains three unique C-terminal residues, GPA, derived from an alternatively spliced C-terminal exon (Wu and Chiang, 2007).

BET inhibitors (BETi) are in pre-clinical and clinical trials for the treatment of various cancers (Filippakopoulos and Knapp, 2014). Targeted inhibition of BRD4 suppresses tumour growth in breast and prostate cancer, as well as in acute myeloid leukaemia and diffuse large B-cell lymphoma (Zuber et al, 2011; Chapuy et al, 2013; Asangani et al, 2014; Shu et al, 2016). Despite its success, BETi therapy is associated with acquired resistance upon prolonged treatment with the inhibitors (Kurimchak et al, 2016). In addition, recent studies have highlighted that BRD4-S and BRD4-L function in an opposing manner in triple-negative breast cancer (TNBC) by differential enhancer regulation of many gene networks, including the matrisome extracellular matrix (ECM) network (Wu et al, 2020). This highlights the importance of developing more target-selective BET inhibitors in cancer therapy.

Previous studies have identified the involvement of BRD4 in RMS. In FP-RMS, BETi JQ1 was found to disrupt PAX3-FOXO1 and BRD4 interaction, leading to degradation of the fusion protein (Gryder et al, 2017). JQ1 reduces RMS tumour growth through anti-angiogenic mechanisms (Bid et al, 2016). The effect of JQ1 was directly proportional to the expression of MYC, regardless of whether the tumour was of embryonal or alveolar origin (Marchesi et al, 2022). In addition, a combination of BRD4 and PLK1 inhibitors showed synergistic anti-tumour effects in paediatric tumour models including RMS that is associated with MYCN-driven gene expression. Similarly, combined inhibition of BET proteins and metabolic tumour driver, mTORC1/2, was found to abrogate RMS growth (Srivastava et al, 2022). Despite growing evidence for a role of BRD4 in RMS, surprisingly, a functional distinction of the BRD4 isoforms in RMS remains elusive.

In this study, we examined the role of BRD4-L and BRD4-S in RMS. We show that BRD4-L and BRD4-S isoforms are both expressed in RMS cell lines and each isoform has a distinct role in tumour progression and metastasis. Transcriptomic and functional analysis in ERMS demonstrate that BRD4-L promotes proliferation and inhibits myogenic differentiation at least in part through regulation of myostatin. Interestingly, BRD4-S functions as a gatekeeper of BRD4-L in metastasis. When BRD4-S is depleted, metastasis is significantly enhanced and BRD4-L enrichment is apparent on several integrin gene promoters. In ARMS, BRD4-L is unrestrained in its oncogenic function. Taken together, the results of this study highlight that BRD4 isoforms have specific functions in RMS.

Results

BRD4 is overexpressed in RMS

Expression of BRD4-long (BRD4-L) and BRD4-short (BRD4-S) isoforms (Fig. 1A) in patient-derived ERMS cell lines—RD, RD18 and JR1. An increased expression of both BRD4 isoforms was seen in all cell lines compared to primary human skeletal muscle myoblasts (HSMM) at the mRNA and protein level (Fig. 1B–D). Immunohistochemical analysis with an anti-BRD4 antibody that detects both isoforms showed that BRD4 expression was elevated in 21 ERMS samples compared to 8 normal muscles in a tissue microarray (TMA) (Fig. 1E). Similarly, BRD4 expression was elevated in 6 archival ERMS tumour sections (Fig. 1G). Weak staining was observed in 35.54% of ERMS TMA samples and 33.33% of ERMS patient tumours, while moderate or strong staining was evident in 65.46% of ERMS TMA samples and 66.66% of ERMS patient tumours (Fig. 1F,H and Appendix Fig. S1). To analyse the relative expression of BRD4-L and BRD4-S RNA transcripts in ERMS tumour sections, we used RNAscope analysis. Quantification of the number of puncta for each isoform revealed that BRD4-S transcripts were more abundant compared to BRD4-L transcripts (Fig. 1I).

BRD4-L and BRD4-S isoforms have distinct roles in tumour progression and metastasis

RMS cells are sensitive to the pan-BRD4 inhibitor JQ1 (Marchesi et al, 2022). We tested the impact of JQ1 treatment in RD cells. A significant decrease in proliferation (Fig. 2A) and an increase in myogenic differentiation cells along with MYOG and MHC expression was seen upon JQ1 treatment compared to DMSO-treated control cells (Fig. 2B,C). Unexpectedly, invasion and migration were significantly increased with JQ1 treatment (Fig. 2D), suggesting that pan-BRD4 inhibition may have an undesired outcome.

To examine whether this outcome was due to distinct roles of the two main BRD4 isoforms, BRD4-L and BRD4-S were individually silenced by stable knockdown in RD cells (Fig. 2E).

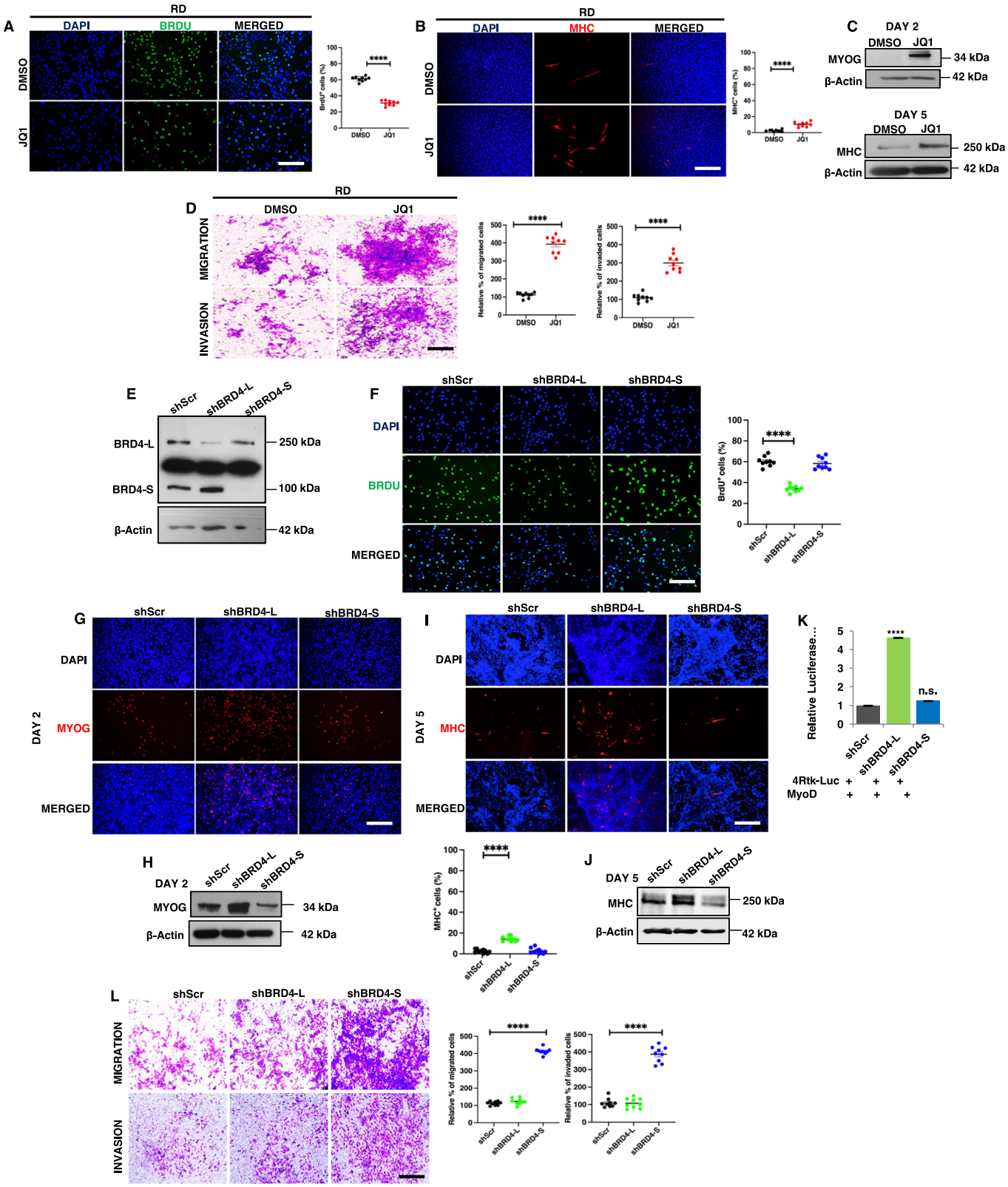
A
RD
DAPI
BRDU
MERGED
DMSO
JQ1
****
BrdU+ cells (%)
B
RD
DAPI
MHC
MERGED
DMSO
JQ1
****
MHC+ cells (%)
C
DAY 2
DMSO JQ1
MYOG
β-Actin
34 kDa
42 kDa
DAY 5
DMSO JQ1
MHC
β-Actin
250 kDa
42 kDa
D
RD
DMSO
JQ1
MIGRATION
INVASION
****
Relative % of migrated cells
****
Relative % of invaded cells
E
shScr
shBRD4-L
shBRD4-S
BRD4-L
BRD4-S
β-Actin
250 kDa
100 kDa
42 kDa
F
shScr
shBRD4-L
shBRD4-S
DAPI
BRDU
MERGED
****
BrdU+ cells (%)
G
shScr
shBRD4-L
shBRD4-S
DAPI
DAY 2
MYOG
MERGED
I
shScr
shBRD4-L
shBRD4-S
DAPI
DAY 5
MHC
MERGED
K
Relative Luciferase...
****
n.s.
shScr
shBRD4-L
shBRD4-S
4Rtk-Luc + + +
MyoD + + +
H
DAY 2
shScr
shBRD4-L
shBRD4-S
MYOG
β-Actin
34 kDa
42 kDa
****
MHC+ cells (%)
J
DAY 5
shScr
shBRD4-L
shBRD4-S
MHC
β-Actin
250 kDa
42 kDa
L
shScr
shBRD4-L
shBRD4-S
MIGRATION
INVASION
****
Relative % of migrated cells
****
Relative % of invaded cells

Figure 2. BRD4-L and BRD4-S have distinct roles in tumour growth and metastasis.

(**A**) RD cells were treated with DMSO (vehicle) or 50 nM of JQ1 for 48 h and proliferation was assessed using BrdU assay by immunofluorescence using anti-BrdU antibody. Nuclei were stained with DAPI (blue). Images are representative of at least three biological replicates. Scale bar: 100 μm. Scatter plot representing the percentage of $BrdU^+$ cells in RD cells treated with DMSO or JQ1. Values correspond to the average ± SEM ($n = 3$ biological replicates with 3 technical replicates shown). Two-tailed non-parametric unpaired t test was performed for statistical analysis. ****$p \leq 0.0001$. (**B**) RD cells were pretreated with 50 nM JQ1 in growth medium and then differentiated with DMSO or JQ1 for 5 days and analysed by immunofluorescence using anti-MHC antibody. Images are representative of at least three biological replicates. Scale bar: 100 μm. Scatter plot representing percentage of MHC^+ cells in DMSO and JQ1-treated RD cells. The values correspond to average ± SEM ($n = 3$ biological replicates with 3 technical replicates shown). Two-tailed non-parametric unpaired t test was performed for statistical analysis. ****$p \leq 0.0001$. (**C**) Western blot analysis using anti-MYOG antibody and anti-MHC antibody in RD cells treated with DMSO or JQ1 in differentiation media for 2 and 5 days, respectively. β-Actin was used as loading control. (**D**) Migratory and invasive capacity of RD cells treated with 50 nM of JQ1 for 48 h was assessed using transwell assays followed by crystal violet staining of the inserts. Images are representative of at least three biological replicates. Scale bar: 100 μm. Scatter plot representing the percentage of migration and invasion of RD cells treated with DMSO or JQ1. The values correspond to average ± SEM ($n = 3$ biological replicates with 3 technical replicates shown). Two-tailed non-parametric unpaired t test was performed for statistical analysis. ****$p \leq 0.0001$. (**E**) Stable knockdown of BRD4-L (shBRD4-L) and BRD4-S (shBRD4-S) in RD cells was analysed using Western blotting. β-Actin was used as loading control. Images are representative of at least three biological replicates. (**F**) Proliferation was assessed using BrdU assay in shScr, shBRD4-L and shBRD4-S RD cells by immunofluorescence using anti-BrdU antibody. Nuclei were stained with DAPI. Images are representative of at least three biological replicates. Scale bar: 100 μm. Scatter plot representing the percentage of $BrdU^+$ cells in shBRD4-L and shBRD4-S compared to shScr cells. The values correspond to average ± SEM ($n = 3$ biological replicates with 3 technical replicates shown). Two-tailed non-parametric unpaired t test was performed for statistical analysis. ****$p \leq 0.0001$. (**G**) shScr, shBRD4-L and shBRD4-S cells were cultured in differentiation media for 2 days and analysed by immunofluorescence using anti-MYOG antibody. Nuclei were stained with DAPI. Images are representative of at least three biological replicates. Scale bar: 100 μm. (**H**) Western blot analysis of MYOG at Day 2 in shBRD4-L and shBRD4-S compared to shScr after culturing cells in differentiation media. (**I**) shScr, shBRD4-L and shBRD4-S cells were cultured in differentiation media for 5 days and analysed by immunofluorescence using anti-MHC antibody. Nuclei were stained with DAPI. Images are representative of at least three biological replicates. Scale bar: 100 μm. Scatter plot representing percentage of MHC^+ cells in shBRD4-L and shBRD4-S cells compared to control cells. The values correspond to average ± SEM ($n = 3$ biological replicates with 3 technical replicates shown). Two-tailed non-parametric unpaired t test was performed for statistical analysis. ****$p \leq 0.0001$. (**J**) Western blot analysis of MHC at Day 5 in shBRD4-L and shBRD4-S compared to shScr after culturing cells in differentiation media. β-Actin was used as loading control. (**K**) MyoD reporter activity was analysed in shScr, shBRD4-L and shBRD4-S cells by transfecting cells with 200 ng of the MRF reporter 4Rtk-luc, 200 ng MyoD and 5 ng Renilla. Luciferase activity was analysed 48 h post transfection. The bar graph represents the average ± SEM ($n = 4$ biological replicates). Two-tailed non-parametric unpaired t test was performed for statistical analysis. ****$p \leq 0.001$, n.s. not significant. (**L**) Migratory and invasive capacity of shScr, shBRD4-L and shBRD4-S cells was assessed using transwell assays followed by crystal violet staining of the inserts. Images are representative of at least three biological replicates. Scale bar: 100 μm. Scatter plot representing the percentage of migration and invasion of shScr, shBRD4-L and shBRD4-S cells. The values correspond to average ± SEM ($n = 3$ biological replicates with 3 technical replicates shown). Two-tailed non-parametric unpaired t test was performed for statistical analysis. ****$p \leq 0.0001$. Source data are available online for this figure.

A significant decrease in the percentage of $BrdU^+$ cells was apparent only in shBRD4-L cells compared to control shScr cells with no significant change in shBRD4-S cells (Fig. 2F). Similar results were observed with transient knockdown of the two isoforms in RD, RD18 and JR1 cell lines (Fig. EV1). An increase in myogenin $(MYOG)^+$ and myosin heavy chain $(MHC)^+$ cells along with MYOG and MHC expression was seen only in shBRD4-L cells compared to shScr, with no overt difference in shBRD4-S cells (Fig. 2G–J). Similar results were observed with a siRNA approach in RD, RD18 and JR1 cell lines (Fig. EV2). Consistent with increased differentiation, shBRD4-L cell lines had a significantly high MyoD activity compared to shScr and shBRD4-S cells (Fig. 2K). Interestingly, a significant increase in migratory and invasive capacity was apparent only in shBRD4-S cells compared to shScr and shBRD4-L cells. A similar outcome was seen with siBRD4-S in RD, RD18 and JR1 cells (Figs. 2L and EV3). These results demonstrate that BRD4-L promotes proliferation and inhibits myogenic differentiation, while BRD4-S inhibits migration and invasion of ERMS cells.

To examine if the isoforms have similar or distinct roles in the two main RMS subtypes, we examined the expression and function of BRD4 isoforms in ARMS. BRD4 expresion was upregulated in ARMS cell lines RH30 and RH41 (Appendix Fig. S2A) and ARMS TMA (Appendix Fig. S2B) with weak staining in 42.76%, and moderate/strong staining in 57.23% samples (Appendix Fig. S2C). BRD4-L and BRD4-S isoforms were transiently silenced in RH30 and RH41 cells (Appendix Fig. S3A,B). BRD4-L knockdown resulted in a significant decrease in proliferation in both cell lines, while BRD4-S knockdown showed no significant impact (Appendix Fig. S3C,D). Myogenic differentiation remained largely unaffected by either isoform (Appendix Fig. S3E–H). Interestingly, cell motility was significantly reduced only in siBRD4-L cells compared to siScr (Control) (Appendix Fig. S3I,J) indicating that BRD4-L, and not BRD4-S, plays a central role in proliferation and motility of ARMS cells. Upon JQ1 treatment in RH30 cells, proliferation was reduced with no significant change in myogenic differentiation (Appendix Fig. S4A,B). However, invasion and migration were increased in response to JQ1 treatment (Appendix Fig. S4C). These findings demonstrate that BRD4-L and BRD4-S have different functions in ERMS and ARMS. Since BRD4-S exhibited a role only in ERMS, we focused subsequent studies on this subtype.

To validate the differential roles in ERMS cells in vivo, RD control (shScr), shBRD4-L or shBRD4-S cells were injected subcutaneously in BALB/c nude mice. The tumour volume was similar between mice injected with shBRD4-S cells and shScr cells (Fig. 3A,B). On the other hand, a significant reduction in tumour volume was seen for the shBRD4-L group and tumours from only four mice could be resected. No adverse effect on the weight of the mice was noted in any group (Fig. 3C). We then tested the impact of the BRD4 isoforms in metastasis. Control shScr, shBRD4-L and shBRD4-S cells were injected into NOD/SCID mice through the tail vein. The control and shBRD4-L group showed a similar number of tumours in the liver. On the other hand, mice injected with shBRD4-S cells showed a strikingly higher number and size of nodules primarily in the liver but also in the kidney, stomach and lungs (Fig. 3D,E). No apparent difference was observed in the body weight of any group (Fig. 3F). The liver, lung and kidney nodules were analysed histologically. Widespread metastasis in the liver, lungs and kidney was apparent in mice injected with shBRD4-S cells compared to control and shBRD4-L group (Appendix Fig. S5).

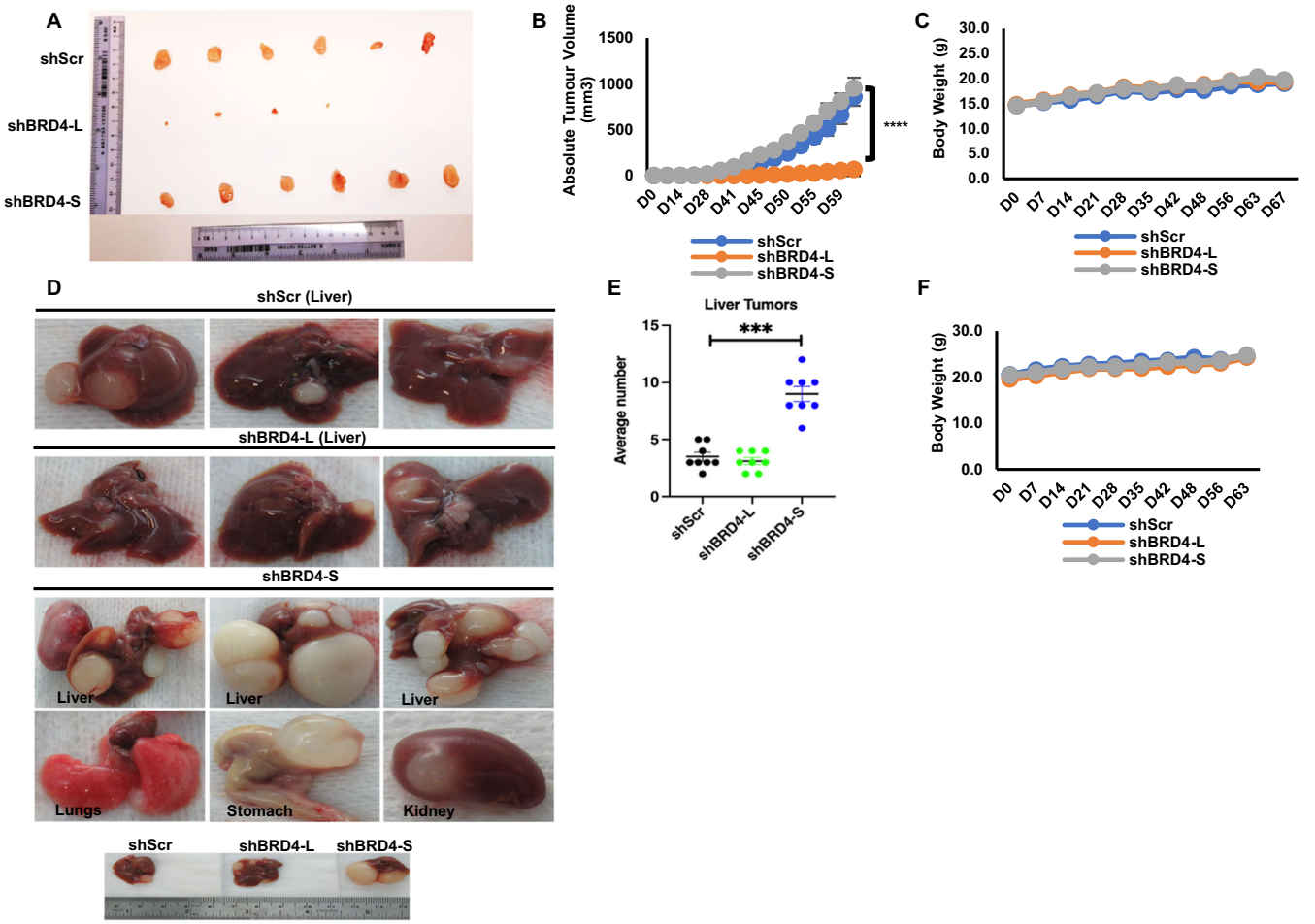

J

DIFFERENTIALLY EXPRESSED GENES (WT VS BRD4-L)	FOLD CHANGE	P-ADJ
Myostatin (*MSTN*)	-1.53	1.36E-29
MyoD Family Inhibitor (*MDFI*)	-1.24	0.0001451
Myosin 1C (*MYO1C*)	1.34	6.55E-16
Myosin9A (*MYO9A*)	1.23	0.00021
Myosin9B (*MYO9B*)	1.27	3.31E-13
Myosin Light Chain 1 (*MYL1*)	1.43	4.67E-13
Myosin Light Chain 5 (*MYL5*)	1.2	0.03
Myosin Light Chain 12A (*MYL12A*)	1.36	4.72E-25

K

DIFFERENTIALLY EXPRESSED GENES (WT VS BRD4-S)	FOLD CHANGE	P- ADJ
Integrin alpha 1 (*ITGA1*)	1.42	2.89E-13
Integrin alpha 4 (*ITGA4*)	1.33	3.95E-12
Integrin beta 5 (*ITGB5*)	1.24	1.47E-05
Integrin alpha 5 (*ITGA5*)	1.21	6.74E-07
Integrin alpha 3 (*ITGA3*)	1.20	0.032811
Cell-Adhesion Associated, Oncogene Regulated (*CDON*)	-1.5	1.19E-27
Junctional Adhesion Molecule 3 (*JAM3*)	-2.29	3.44E-127
Metastasis Suppressor 1 (*MTSS1*)	-1.26	0.03

Figure 3. BRD4-L enhances tumour growth whereas BRD4-S blocks metastasis in vivo.

(A) Nude mice ($n = 10$/group) were injected with shScr, shBRD4-L and shBRD4-S cells to analyse tumour growth. Tumours were resected from 6 shScr and shBRD4-S mice and from 4 shBRD4-L mice. **(B,C)** The graphs represent absolute tumour volume **(B)** and average body weight **(C)** of mice. Statistical significance was calculated using repeated-measure one-way ANOVA where ****$p \leq 0.0001$. Values correspond to the average ± SEM ($n = 10$/group). **(D)** NOD/SCID mice were injected through the tail vein with shScr, shBRD4-L and shBRD4-S cells ($n = 10$/group). Metastasis was seen in the liver for shScr and shBRD4-L groups, while tumours were seen in the liver, lungs, stomach and kidney in shBRD4-S group. **(E)** Scatter plot representing the average number of liver nodules in mice injected with shScr, shBRD4-L and shBRD4-S cells. Values correspond to the average ± SEM. Two-tailed non-parametric unpaired t test was performed for statistical analysis. ***$p \leq 0.001$. **(F)** Graph representing average body weights of control shScr, shBRD4-L, shBRD4-S mice. Values correspond to the average ± SEM ($n = 10$/group). **(G)** Heat map indicates hierarchical cluster of differentially expressed genes (DEGs) between control siScr (BRD4_WT), siBRD4-L and siBRD4-S RD cells. Red and blue colours represent high and low expression of genes, respectively. **(H,I)** Volcano plot and pie charts indicate the distribution and number of upregulated and downregulated genes in siBRD4-L versus control (WT) and siBRD4-S compared to siScr control (WT) groups ($n = 1$ biological replicate with 3 technical replicates). **(J)** A list of the top significantly altered genes related to myogenesis in the siBRD4-L vs siScr group is shown with the fold change and *p*-adjusted values. Differential gene expression analysis was conducted using the DESeq2 package, with statistical significance determined by a corrected *p* value (p-adjusted) <0.05 and fold change >1.2. **(K)** A list of the top significantly altered genes related to migration and invasion identified in the siBRD4-S vs siScr group with the fold change and *p*-adjusted values. Differential gene expression analysis was conducted using the DESeq2 package, with statistical significance determined by a corrected *p* value (p-adjusted) <0.05 and fold change >1.2. Source data are available online for this figure.

BRD4-L and BRD4-S regulate distinct target genes

To identify the mechanisms underlying their distinct roles, we performed RNA-sequencing analysis using three technical replicates of siScr, siBRD4-L and siBRD4-S RD cells. Hierarchical cluster analysis of differentially expressed genes (DEGs) and volcano plots showed that 2974 and 692 genes were differentially regulated in siBRD4-L and siBRD4-S cells, respectively, when compared to BRD4_WT (Fig. 3G–I and Dataset EV1). 1370 genes were upregulated while 1604 genes were downregulated in siBRD4-L cells (Fig. 3H). 308 genes were upregulated and 384 genes were downregulated in siBRD4-S cells (Fig. 3I). Gene Ontology (GO) analysis showed that cell-substrate adherens junction, focal adhesion and actin cytoskeleton were upregulated in siBRD4-L cells that are important for cellular differentiation. Similarly, cell-substrate adherens junction, and focal adhesion were upregulated with siBRD4-S cells correlating with cell motility (Fig. EV4A). In corroboration with the phenotypic effects, myogenic differentiation genes were modulated upon BRD4-L knockdown. Several genes, including *MSTN, MDFI*, were downregulated while *MYO1C, MYO9A, MYO9B, MYL1, MYL5* and *MYL12A* were upregulated on silencing BRD4-L (Fig. 3J). In contrast, upon BRD4-S knockdown, a distinct set of genes that promote migration and invasion including integrins *ITGA1* (Gharibi et al, 2017), *ITGA3* (Jiao et al, 2019), *ITGA4* (Pulkka et al, 2018), *ITGA5* (Li et al, 2022) were upregulated while some metastasis-suppressors like *CDON, MTSS1* and *JAM3* were downregulated (Fig. 3K). We validated some of the targets regulated by BRD4-L and BRD4-S by RT-qPCR. The mRNA level of *MSTN* was downregulated while *MYL12A* and *MYL5* were upregulated in siBRD4-L cells compared to siScr and siBRD4-S cells (Fig. EV4B). On the other hand, expression of *ITGA1*, *ITGA3*, *ITGA4* and *ITGA5* was upregulated in siBRD4-S cells compared to siScr and siBRD4-L cells (Fig. EV4C).

BRD4-L regulates myogenic differentiation through myostatin

Among the genes that were downregulated upon BRD4-L knockdown, we were particularly interested in myostatin (*MSTN*) that is a negative regulator of myogenic differentiation in RMS cells (Ricaud et al, 2003). Myostatin protein was downregulated in shBRD4-L cells compared to shScr and shBRD4-S cells (Fig. 4A). Moreover, tumour lysates from two independent mice from the xenograft assays showed that MHC levels were elevated and myostatin levels were significantly reduced in shBRD4-L tumours compared to shScr control and shBRD4-S tumours (Fig. 4B). To examine whether BRD4-L directly regulates myostatin, we examined BRD4-L occupancy at the myostatin promoter using ChIP-qPCR. A significant occupancy of BRD4-L was seen at the myostatin promoter with no enrichment of BRD4-S (Fig. 4C). Moreover, enrichment of the activation mark H3K9Ac (Fig. 4D) along with RNA Pol II (Fig. 4E) was seen. No significant change in enrichment of BRD4-L and RNA Pol II was seen in shBRD4-S cells compared to control cells (Fig. 4F,G).

To confirm that myostatin is a downstream effector of BRD4-L, we added exogenous recombinant myostatin protein to shBRD4-L cells. Addition of myostatin increased proliferation in shBRD4-L cells (Fig. 4H). A modest decrease in proliferation in shScr and shBRD4-S cells was apparent on addition of myostatin. Myostatin also reversed the enhanced myogenic differentiation seen in shBRD4-L cells (Fig. 4I) that was evident by the decrease in MHC^+ cells and by western blot analysis (Fig. 4J).

An interplay between BRD4-S and BRD4-L is involved in the regulation of integrin genes

Several integrin genes (*ITGA1, ITGA3, ITGA4, ITGA5, ITGB5*) were significantly upregulated upon knockdown of BRD4-S (Figs. 3K and EV4C). We validated ITGA4 and ITGA5 protein expression in shBRD4-S cells compared to shBRD4-L and shScr control cells (Fig. 5A). Additionally, a remarkably high expression of ITGA4 and ITGA5 was seen in the liver nodules isolated from two independent shBRD4-S mice from the in vivo metastasis experiments (Fig. 5B). Since BRD4 mostly functions as an activator, we examined how loss of BRD4-S could result in an upregulation of integrin genes. A higher enrichment of BRD4-S compared to BRD4-L was apparent at *ITGA4* and *ITGA5* genes (Fig. 5C). A significant enrichment of H3K9Ac was also seen at the promoters of *ITGA4* and *ITGA5* (Fig. 5D) although occupancy of RNA Pol II was not observed (Fig. 5E).

Previous studies have demonstrated that a BRD4-S-like activity via deletion of the proline-rich region in BRD4-L may oppose the function of BRD4-L by competing for target acetyl lysine residues (Alsarraj et al, 2011). We therefore examined if BRD4-S inhibits binding of BRD4-L at the integrin gene promoters. Interestingly, in the shBRD4-S cells, an increase in BRD4-L enrichment was seen,

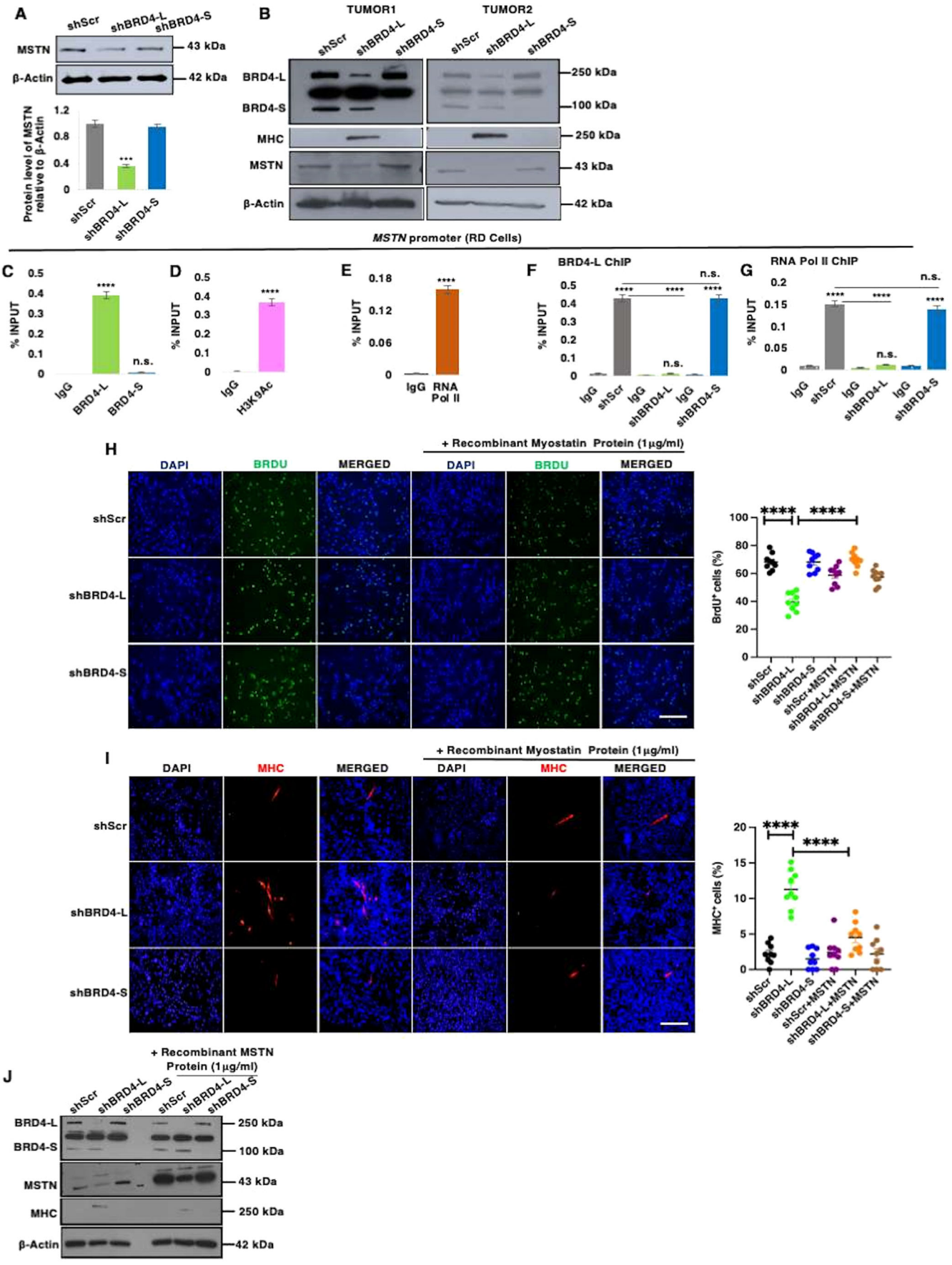
A
shScr
shBRD4-L
shBRD4-S
MSTN
43 kDa
β-Actin
42 kDa
Protein level of MSTN relative to β-Actin
B
TUMOR1
TUMOR2
BRD4-L
BRD4-S
250 kDa
100 kDa
MHC
MSTN
β-Actin
MSTN promoter (RD Cells)
C
% INPUT
IgG
BRD4-L
BRD4-S
n.s.
D
H3K9Ac
E
RNA Pol II
F
BRD4-L ChIP
G
RNA Pol II ChIP
H
+ Recombinant Myostatin Protein (1μg/ml)
DAPI
BRDU
MERGED
BrdU+ cells (%)
shScr+MSTN
shBRD4-L+MSTN
shBRD4-S+MSTN
I
MHC
MHC+ cells (%)
J
+ Recombinant MSTN Protein (1μg/ml)

Figure 4. BRD4-L promotes proliferation and represses myogenic differentiation via regulation of MSTN expression.

(A) MSTN protein level was analysed in shScr, shBRD4-L and shBRD4-S cells. β-Actin was used as loading control. Images are representative of at least three biological replicates. Densitometric analysis was done to quantify MSTN expression relative to β-Actin from three independent experiments and is shown in the bar graph. Error bars correspond to the average ± SEM ($n = 3$ biological replicates). Two-tailed non-parametric unpaired t test was performed for statistical analysis. ***$p \leq 0.001$. **(B)** Tumour lysates from 2 independent RD shScr, shBRD4-L and shBRD4-S xenografts were analysed for BRD4, MHC and MSTN expression using Western blotting. β-Actin was used as loading control. **(C–E)** ChIP assay was performed to examine the enrichment of BRD4-L and BRD4-S isoforms **(C)**, H3K9Ac **(D)** and RNA Pol II **(E)** on the *MSTN* promoter relative to IgG control. The values were plotted as percentage of input, the average ± SEM is shown (n = 4 biological replicates). Two-tailed non-parametric unpaired t test was performed for statistical analysis. ****$p \leq 0.0001$. **(F,G)** ChIP assay to examine the enrichment of BRD4-L **(F)** and RNA Pol II **(G)** in shBRD4-L and shBRD4-S compared to shScr control cells on MSTN promoter. The values were plotted as percentage of input, average ± SEM ($n = 4$ biological replicates). Two-tailed non-parametric unpaired t test was performed for statistical analysis. ****$p \leq 0.0001$, n.s. not significant. **(H)** BrdU assay in shScr, shBRD4-L and shBRD4-S cells and treated with or without 1 µg/ml of recombinant myostatin protein for 72 h. Nuclei were stained with DAPI (blue). Images are representative of at least three biological replicates. Scale bar: 100 µm. Scatter plot showing the percentage of $BrdU^+$ cells in shBRD4-L, shBRD4-S in comparison with shScr cells treated with or without recombinant myostatin protein. The values correspond to the average ± SEM ($n = 3$ biological replicates with 3 technical replicates shown). Statistical significance was calculated by one-way ANOVA analysis. ****$p \leq 0.0001$. **(I)** shScr, shBRD4-L and shBRD4-S cells were cultured in differentiation media in the absence or presence of 1 µg/ml of recombinant myostatin protein for 72 h. MHC^+ cells were analysed by immunofluorescence with anti-MHC antibody. Images are representative of at least three biological replicates. Scale bar: 100 µm. Scatter plot indicating MHC^+ cells in shBRD4-L, shBRD4-S in comparison with shScr cells with or without recombinant myostatin protein. The values correspond to the average ± SEM ($n = 3$ biological replicates with 3 technical replicates shown). Statistical significance was calculated by one-way ANOVA analysis. ****$p \leq 0.0001$. **(J)** Western blot analysis indicating protein expression of MHC and MSTN in shScr, shBRD4-L and shBRD4-S cells with or without recombinant myostatin protein for 72 h. β-Actin was used as loading control. Source data are available online for this figure.

indicating that reduction in BRD4-S allows for elevated BRD4-L occupancy (Fig. 5F). Notably, there was no significant change in BRD4-S enrichment in shBRD4-L cells compared to shScr control cells (Fig. 5G). In addition to elevated BRD4-L occupancy, there was also enrichment of RNA Pol II in shBRD4-S cells, indicating an assembly of a transcription complex (Fig. 5H).

To confirm whether BRD4-L drives expression of integrin genes and cellular motility in the absence of BRD4-S, we silenced BRD4-L using siRNA in the shBRD4-S cells. Interestingly, the migratory and invasive capacity of the shBRD4-S plus siBRD4-L cells was reduced to that of shScr cells (Fig. 5I). Western blot analysis revealed that expression of ITGA4 and ITGA5 in shBRD4-S cells transfected with siBRD4-L was similar to that of shScr control cells (Fig. 5J). To confirm whether ITGA4 and ITGA5 are key targets involved in increased migration and invasion of shBRD4-L cells, we transiently knocked down their expression individually or together in shScr, shBRD4-L and shBRD4-S cells. Depletion of ITGA4 or ITGA5 individually partially reversed the phenotype of shBRD4-S cells, but the reduction was very pronounced when both genes were silenced in shBRD4-S cells (Fig. EV5A–C). Consistent with enhanced cell motility, c-Myc and Zeb2 that regulate metastasis (Wolfer et al, 2011; Brabletz et al, 2021) were upregulated in shBRD4-S cells compared to shScr and shBRD4-L cells (Fig. EV5D).

Collectively, our data support a model where BRD4-L is involved in tumour progression and inhibits differentiation of ERMS cells, at least in part, by regulation of myostatin. BRD4-S, on the other hand, acts as a gatekeeper. Removal of the blockade imposed by BRD4-S permits BRD4-L to promote metastasis by regulating expression of integrin genes (Fig. EV5E).

Discussion

In this study, we provide the first evidence for distinct isoform-specific roles of BRD4 in ERMS. We demonstrate that BRD4-L represses MyoD activity and myogenic differentiation. On the other hand, intriguingly, BRD4-S limits the oncogenic role of BRD4-L by acting as a gatekeeper of metastasis. In the absence of BRD4-S, significant enrichment of BRD4-L as well as RNA Pol II is apparent on integrin gene promoters, resulting in their elevated expression that correlates with increased metastasis.

Early studies in breast cancer showed that BRD4 functions as a tumour suppressor and its overexpression in a MYC-driven murine mammary tumour cell line reduces breast cancer growth in vivo (Crawford et al, 2008; Alsarraj et al 2011). BRD4 also mediates resistance to transformation in patients with Hutchinson Gilford Progeria Syndrome (Fernandez et al, 2014). In contrast, BRD4 is overexpressed in various cancers including triple-negative breast cancer where it promotes oncogenesis (Stathis and Bertoni, 2018; Donati et al, 2018) largely, though not exclusively through MYC family members (Delmore et al, 2011; Slavish et al, 2020; Lenhart et al, 2015). Consequently, pan-BET inhibitors (BETi) show promising anti-tumour activity in diverse pre-clinical models albeit with some limitations (Zuber et al, 2011; Shu et al, 2016; Cheng et al, 2013). For instance, sustained JQ1 treatment results in acquired resistance in ovarian cancer (Kurimchak et al, 2016). In addition, while JQ1 is effective in inhibition of prostate cancer growth, it promotes metastasis (Wang et al 2020). Similarly, in breast cancer, I-BET151 is effective in inhibiting primary tumour growth, but does not impact metastasis (Alsarraj et al, 2013). Some of these undesired effects of BETi could be a consequence of targeting other BET proteins (BRD2 and BRD3) that can have opposing functions (Andrieu and Denis, 2018). In addition, the two BRD4 isoforms have antagonistic roles in tumour progression and metastasis in breast cancer where BRD4-S functions as an oncogene, while BRD4-L acts as a tumour suppressor (Wu et al, 2020; Alsarraj et al, 2011). Unlike breast cancer, where BRD4-L functions as a tumour suppressor, in ERMS and ARMS, it appears to have an oncogenic role indicating context-specific roles. These apparently opposing functions in breast cancer and RMS may be related to the origins, somatic mutation burden, and epigenetic landscapes that are distinct in adult and paediatric cancers. Moreover, the relative expression of BRD4-L and BRD4-S in different cancers may determine their functional requirement in different cellular contexts. It is noteworthy that the BRD4 isoforms have different roles in ERMS and ARMS. In ARMS, BRD4-L is unrestrained in its oncogenic role as BRD4-S does not appear to be involved. The differential functions of BRD4-L and BRD4-S in these two subtypes may relate to the molecular heterogeneity of

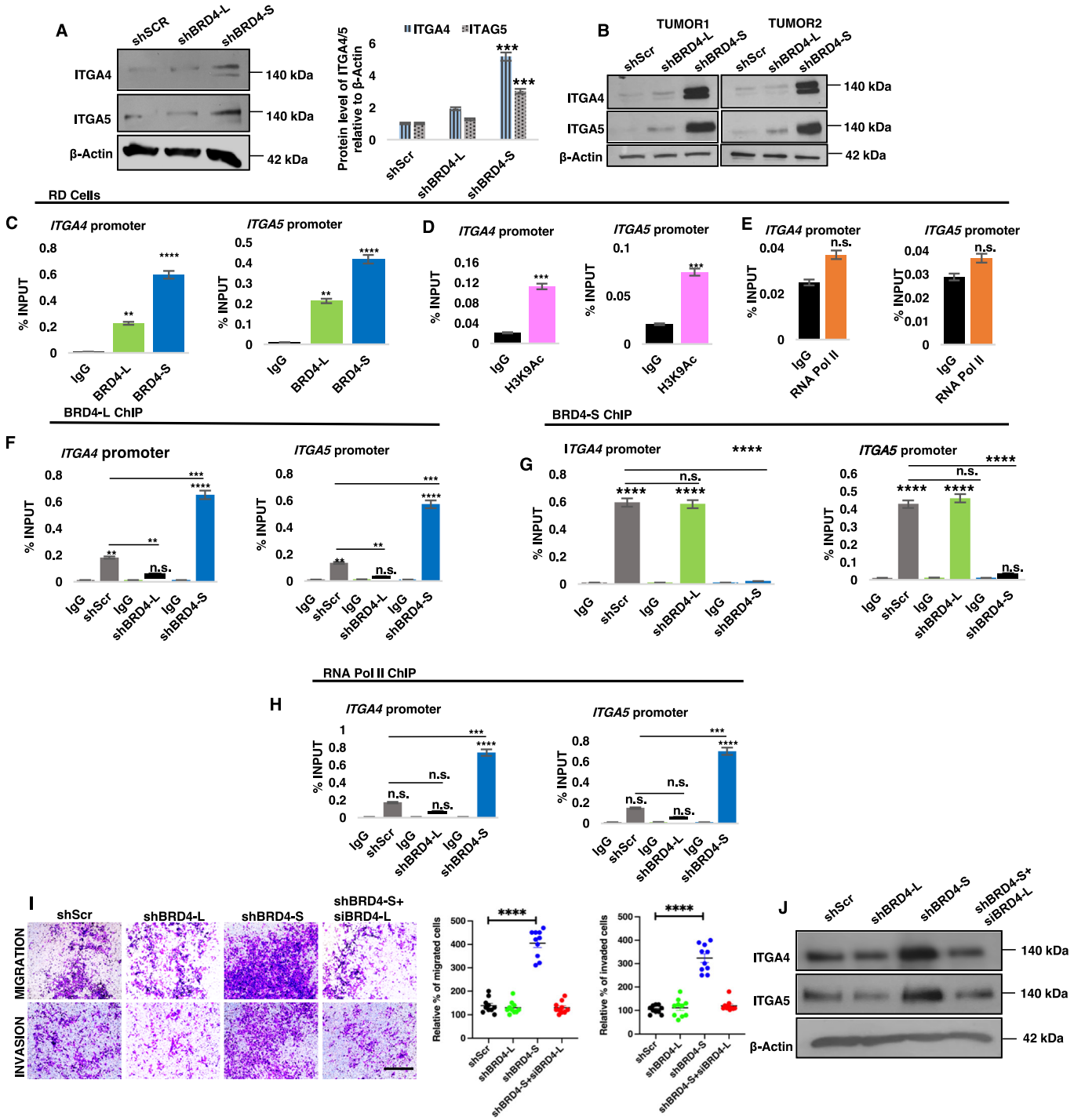

ERMS and ARMS (Skapek et al, 2019). As JQ1 increases motility in both subtypes, our data suggest that BRD2/3 function could also be important in RMS. The subtype and cancer-specific roles underscore the need to systematically dissect BRD4 isoform-specific functions and BET protein functions for precision targeting in disease therapy.

Our data demonstrate that BRD4-L regulates differentiation at least in part through regulation of myostatin. Myostatin is a well-established negative regulator of myogenesis and inhibitor of MyoD activity. Myostatin has previously been shown to inhibit proliferation of RMS cells, and its suppression with a dominant negative form of activin receptor type IIb promotes differentiation. BRD4 interacts with the methyltransferase SMYD3 to regulate myostatin expression (Proserpio et al, 2013). On the other hand, our functional and transcriptomic data demonstrate that BRD4-S loss enhances expression of integrins due to increased BRD4-L binding to integrin gene promoters. These findings are consistent with previous studies which demonstrated that a BRD4-S-mimicking activity may compete with BRD4-L for binding to

Figure 5. Integrins are downstream targets of BRD4-S.

(**A**) Western blot analysis of ITGA4 and ITGA5 in shScr, shBRD4-L and shBRD4-S cells. β-Actin was used as loading control. Images are representative of at least three biological replicates. ITGA4 and ITGA5 expression relative to β-Actin from three independent experiments was quantified densitometrically and is shown in the bar graph. Error bars correspond to the average ± SEM ($n = 3$ biological replicates). Two-tailed non-parametric unpaired t test was performed for statistical analysis. ***$p \leq 0.001$. (**B**) Tumour lysates from 2 independent NOD/SCID mice from tail vein assays were analysed for expression of ITGA4 and ITGA5 using Western blotting. β-Actin was used as loading control. (**C**) ChIP assay was performed to examine the enrichment of BRD4-L and BRD4-S on *ITGA4* and *ITGA5* promoter, IgG was used as a control. The values were plotted as percentage of input, average ± SEM ($n = 4$ biological replicates). Two-tailed non-parametric unpaired t test was performed for statistical analysis. **$p \leq 0.01$, ****$p \leq 0.0001$. (**D**,**E**) ChIP assay was performed to examine the enrichment of H3K9Ac (**D**) and RNA Pol II (**E**) on the *ITGA4* and *ITGA5* promoter. The values were plotted as percentage of input, average ± SEM ($n = 4$ biological replicates). Two-tailed non-parametric unpaired t test was performed for statistical analysis. ***$p \leq 0.001$, n.s. = not significant. (**F–H**) Enrichment of BRD4-L (**F**), BRD4-S (**G**) and RNA Pol II (**H**) in shScr, shBRD4-L and shBRD4-S cells at the *ITGA4* and *ITGA5* promoter was analysed by ChIP assay The values were plotted as percentage of input, the average ± SEM ($n = 4$ biological replicates) is shown. Two-tailed non-parametric unpaired t test was performed for statistical analysis. n.s. not significant, **$p \leq 0.01$, ***$p \leq 0.001$ and ****$p \leq 0.0001$. (**I**) Upon transient knockdown of BRD4-L in shBRD4-S cells for 48 h, migratory and invasive capacity of shScr, shBRD4-L and shBRD4-S cells was analysed using transwell assay. The inserts were stained with crystal violet. Images are representative of at least three biological replicates. Scale bar: 100 μm. Scatter plots show the percentage of migrated and invaded shScr, shBRD4-L, shBRD4-S and shBRD4-S + siBRD4-L cells after 48 h. The values correspond to the average ± SEM ($n = 5$ biological replicates with 2 technical replicates shown). Statistical significance was calculated by one-way ANOVA analysis. ****$p \leq 0.0001$. (**J**) Western blot analysis of ITGA4 and ITGA5 in shScr, shBRD4-L, shBRD4-S and shBRD4-S + siBRD4-L. β-Actin was used as loading control. Source data are available online for this figure.

acetylated histones and interferes with BRD4-L function (Alsarraj et al, 2011) likely due to an expanded histone binding of BRD4-S versus BRD4-L.

Our finding that each BRD4 isoform regulates specific gene targets is in line with previous studies (Wu et al, 2020; Han et al, 2020). We identified several integrins which are key players in cellular adhesion and migration (Hamidi and Ivaska, 2018) among the targets that are regulated by BRD4-S. Integrins participate in the remodelling of ECM and colonization of cancer cells in new metastatic sites. N-cadherin and α9-integrin link the Notch pathway to cell adhesion, motility and invasion in RMS (Masià et al, 2012). The BRD4/c-Myc axis also intersects with integrin/FAK-dependent pathway in TNBC (Zhang et al, 2020).

The mechanisms by which the two isoforms regulate specific gene transcription in ERMS cells need further investigation. Isoform-specific binding partners might determine binding specificity and distinct functions of the isoforms. Taken together, our study highlights the value of BRD4-isoform-specific therapeutic strategies in ERMS and indicates that BRD4-S expression may be a biomarker of cancer metastasis.

Methods

Cell lines, BRD4 transient and stable knockdown

ERMS (RD, RD18, JR1) and ARMS (RH30 and RH41) cell lines, were a kind gift by Peter Houghton (Nationwide Children's Hospital, OH, USA) and Rosella Rota (Bambino Gesu Children's Hospital, ROM, IT). The cell lines were routinely tested for mycoplasma contamination using BioMycoX® Mycoplasma PCR Detection Kit (Atlantis Bioscience, SGP). Cell line authenticity was established through Short Tandem Repeats (STR) analysis (Axil Scientific Pte Ltd, SGP). RD cells were maintained in Dulbecco's modified Eagle's medium (DMEM) (Sigma-Aldrich, St. Louis, MO, USA), supplemented with 10% foetal bovine serum (FBS) (HyClone, Cytiva, USA) and 1% Penicillin–Streptomycin (HyClone, Cytiva, USA). RD18, JR1, RH30 and RH41 cells were cultured in RPMI 1640 with L-Glutamine (Thermo Fisher Scientific, Waltham, MA, USA) supplemented with 10% FBS and 1% Penicillin–Streptomycin. Primary human skeletal muscle myoblasts (HSMM) were purchased from Zen-Bio, Inc. (NC, USA) and cultured in skeletal muscle cell growth medium (#SKM-M, Zen-Bio, USA). HEK-293T cells were commercially purchased from American Type Culture Collection (ATCC) (Manassas, VA, USA) and cultured in DMEM supplemented with 10% FBS.

For transient knockdown, cells were transfected with 20 nM of siRNA using Lipofectamine RNAiMax (Thermo Fisher Scientific). Cells were analysed 48 h post transfection. Specific siRNAs for BRD4-L (targeting long variant; Cat. #: SI05044872), BRD4-S (targeting short variant 3′-UTR region; Cat#: SI05044865) and AllStars Negative control (Cat. #: SI03650318) were purchased from QIAGEN (MD, USA). ITGA4 siRNA (Cat. # SC 35685) and ITGA5 siRNA (Cat. # SC 29372) were purchased from Santa-Cruz Biotechnology Inc.

Stable knockdown cell lines were generated using lentiviral vectors. Around 90% confluent HEK-293T cells were transfected with packaging plasmid pIP1 (5 μg) and pIP2 (5 μg), envelope plasmid pIP/VSV-G (5 μg) (ViraPowerTM Lentiviral Packaging Mix, Thermo Fisher Scientific), 5 μg of lentiviral expression construct shRNA (pLKO.1 Mission shRNA DNA clone, Sigma-Aldrich Inc., St. Louis, MO, USA) control, shBRD4-L (#TRCN0000021424, Mission shRNA, Sigma-Aldrich Inc.) or shBRD4-S (#TRCN0000349782, Mission shRNA, Sigma-Aldrich Inc.) along with 30 μl of Lipofectamine 3000 (Thermo Fisher Scientific) following manufacturer's instruction. The supernatant was replaced with Basal DMEM media 16 h post-transfection. Viral pellet was collected and resuspended in DMEM media. RD cells were transduced with control lentiviral particles, shBRD4-L or shBRD4-S with polybrene (8 μg/ml) (Sigma-Aldrich Inc.). Transduced cells were preselected with 1 μg/ml puromycin (Sigma-Aldrich Inc.) for 4–5 days before expansion.

RNAscope assay

RNAscope® Customized Probe-Hs-BRD4-O2 (BRD4-L; NM_058243.2; Target region 3314–4735) and Catalogue Probe-Hs-BRD4-O1 (BRD4-S; NM_014299.2; Target region 2381–3468) were obtained from Advanced Cell Diagnostics, Inc. (Hayward, CA) (Cat. #: 323100). Detection of BRD4-L and BRD4-S isoforms in formalin-fixed paraffin-embedded (FFPE) archival primary ERMS tumours was investigated using RNAscope® Multiplex

Fluorescent v2 Assay following manufacturer's instructions. A negative control (NC) slide provided in the kit was probed with a negative control probe targeting the DapB gene (Cat. #: 320871). Normal skeletal muscle (the normal muscle panel in the tumour microarray) was used as a control. Briefly, sections were deparaffinized, boiled with target retrieval reagents (30 min), digested with protease (40 °C for 30 min) and then hybridized with the probes (40 °C for 2 h). After six rounds of amplification, the probes were visualized with TSA Plus Cyanine3 (used for BRD4-L), and TSA Plus Cyanine5 (used for BRD4-S) (PerkinElmer, MA, USA. Coverslips were mounted with DAPI (Vectashield, Vector Laboratories, CA, USA) and images were acquired at ×40 magnification with a Leica DCF 9000 GT digital camera using a Leica DMi8 microscope. For quantitative microscopical evaluation of control or test probe mRNA detection, QuPath software (v 0.4.1) was used to analyse each fluorophore channel separately and the absolute numbers of puncta were calculated in the separate channels.

Proliferation, differentiation, migration and invasion assays

Proliferation was measured by using 5-bromo-2′-deoxy-uridine (BrdU) labelling and detection kit (Roche, BSL, CH) as described earlier (Pal et al, 2020). Cells were fixed and incubated with anti-BrdU antibody (1:100) after pulsing with 10 μM BrdU. Cells were incubated with anti-mouse Ig-fluorescein antibody (1:200) and mounted on glass slides using DAPI (Vectashield, Vector Laboratories, CA, USA). Images were acquired in ×40 magnification using a fluorescence microscope BX53 (Olympus Corporation, Shinjuku, TYO, JP).

Transient or stable knockdown cells were cultured in differentiation media consisting of either basal DMEM (for RD cells) or RPMI 1640 (for RD18, JR1, RH30 and RH41 cells) with 2% Horse Serum (HyClone, Cytiva, USA) for 2–5 days (3 days for RH30 and RH41) as described (Pal et al, 2020). Cells were fixed with 4% paraformaldehyde, blocked and permeabilized with 10% horse serum and 0.1% Triton X containing PBS. Cells were then incubated with anti-MHC antibody (MHC; R&D Systems, Minneapolis, MN, USA) (1:400), followed by secondary goat anti-Mouse IgG (H + L) Highly Cross-Adsorbed Secondary Antibody, Alexa Fluor 568 (Thermo Fisher Scientific). Coverslips were mounted with DAPI (Vectashield, Vector Laboratories, CA, USA) and images were acquired at ×40 magnification using a fluorescence microscope BX53.

Boyden chamber (Greiner Bio-One, KR, AT) assay was used to assess the migration and invasion as described (Bhat et al, 2019). Cells were serum-deprived for 12 h and 50,000 RD RD18, RH30 and RH41 cells or 30,000 JR1 cells were seeded in serum-free media into the Transwell insert. After 24–30 h, the inserts were stained with crystal violet and imaged at ×10 magnification using a brightfield microscope (EVOS XL Core Imaging System, Thermo Fisher Scientific). Invasion was assessed using inserts coated with Matrigel (Corning, NY, USA) and seeded at a density of 70,000 cells/insert for RD, RD18, RH30 and RH41 cells; and 50,000 JR1 cells.

RNA isolation, RT-qPCR and RNA-sequencing (RNA-Seq)

Total RNA was extracted using Trizol agent (Thermo Fisher Scientific) and quantified by NanoPhotometer (Implen, CA, USA). 2 μg of total RNA was reverse-transcribed to single-stranded complementary DNA (cDNA) using iScript cDNA Synthesis Kit (Bio-Rad Hercules, CA, USA). RT-qPCR was run on Lightcycler 480 (Roche) using SYBR Green 1 Master Kit (Roche). PCR amplification was performed as described (Bhat et al, 2019). CT values were normalized to the internal control GAPDH, and delta CT (ΔCT) values were obtained. Relative expression was calculated by $2^{-\Delta CT}$ equation. RT-qPCR analyses were done in triplicate and each performed in three independent biological replicates. Primers for RT-qPCR are listed in Appendix Table S1.

For RNA-Seq analysis, RD cells were transfected with siScr control, siBRD4-L or siBRD4-S siRNA for 48 h. Total RNA was isolated and purified using RNeasy mini kit (QIAGEN). Quality of purified RNA was analysed using agarose gel electrophoresis and Agilent 2100. The samples were processed by Novogene AIT for complementary DNA (cDNA) library construction and read mapping. The raw image file from Illumina (HiSeq PE150) was transformed to Sequence Reads by CASAVA base recognition and stored in FASTQ (fq) format. Reads were filtered to gather clean reads using filtering conditions like reads without adaptors, reads containing number of bases that cannot be determined below 10% and at least 50% bases of the reads having Qscore denoting Quality value ≤5. For mapping of the reads, STAR software was used (Dobin et al, 2013). 1 M base was used as the sliding window for distribution of the mapped reads. Differentially expressed genes (DEGs), Gene Ontology (GO) and Kyoto Encyclopedia of Genes and Genomes (KEGG) analysis was performed with corrected p value < 0.05 and fold change ≥1.2, as significant enrichment. RNA-Seq data has been deposited in GEO database under accession number GSE215393.

Western blotting

Cells were lysed with RIPA lysis buffer (50 mM Tris HCl pH 7.5, 40 mM NaCl, 1% NP-40, 0.25% sodium deoxycholate, and 1 mM EDTA) containing protease inhibitor cocktail (Complete Mini, Sigma-Aldrich Inc.). Immunoblots were probed overnight with primary antibodies and incubated with relevant horseradish peroxidase (HRP)-conjugated secondary antibodies. The following primary antibodies were used: anti-BRD4 (short and long isoforms) (Cat. #: ab128874, Abcam (CB, UK), WB 1:1000), anti-BRD4 E2A7X (long isoform) (Cat. #: 13440S, CST (MA, USA), WB 1:1000), anti-GDF8/Myostatin (Cat. #: ab201954, Abcam, WB 1/1000), anti-MHC (Cat. #: sc-32732, Santa-Cruz Biotechnology Inc., WB 1:250), anti-MYOG (Cat. #: sc-12732, Santa-Cruz Biotechnology Inc., WB 1/250), anti-ITGA4 (Cat. #: 8440, CST, WB 1:1000), anti-ITGA5 (Cat. #: 4705, CST, WB 1:1000) and anti-β-actin (Cat. #: A2228, WB 1:10,000, Sigma-Aldrich Inc.), anti-Zeb2 (Cat. #: ab138222, Abcam, WB 1/1000) and anti-c-Myc (Cat. #: sc-40, Santa-Cruz Biotechnology Inc., WB 1/500). Appropriate secondary antibodies (IgG-Fc Specific-Peroxidase) of mouse or rabbit origin (Sigma-Aldrich Inc.) were used. Proteins were detected using Pierce ECL Western Blotting Substrate (Thermo Fisher Scientific). Quantification of western blots was done with ImageJ (v1.53t) software. The signal was normalized to β-actin.

Chromatin immunoprecipitation (ChIP)

For standard ChIP-qPCR, 4×10^6 RD, JR1, shBRD4-L, shBRD4-S or shScr control cells were fixed with formaldehyde as described

(Pal et al, 2020). ChIP was conducted with 2 µg of IgG or purified antibodies against BRD4-L (Cat. #: 13440S, CST, 1:50), H3K9Ac (Cat. #: ab4441, Abcam) and RNA Pol II (Ser2P) (Cat. #: ab193468, Abcam) or 1 µg of BRD4-S (Wu et al, 2020) and analysed by qPCR using 4% of IP products and 0.2% of input DNA. Primers for ChIP-qPCR are listed in Appendix Table S2.

Reporter assays

MyoD reporter activity was analysed as described (Ling et al, 2012). shScr, shBRD4-L and shBRD4-S cells were transfected with 200 ng of the MRF-dependent reporter 4Rtk-luc and 200 ng of MyoD in a 24-well plate format. 5 ng of Renilla reporter was co-transfected as an internal control. Transfection was carried out using Lipofectamine 3000 transfection reagent (Thermo Fisher Scientific). Reporter activity was analysed 48 h post-transfection with the Dual-Luciferase Reporter Assay System (Promega, Madison, WI, USA). Luminescence was analysed with a Varioskan plate reader using SkanIT software.

Tissue microarray and immunohistochemistry

Tissue Microarray (TMA) (SO2082b) slides were purchased from US Biomax, Inc. (Derwood, MD, USA), which comprised of 27 ERMS, 24 ARMS tumour specimens and 8 striated muscle tissues. Six paraffin sections of archival primary ERMS tumours (P1–P6) from KK Women's and Children Hospital in Singapore were also analysed. Specimens were obtained following informed written consent under Institutional Review Board-approved protocol CIRB 2014/2079. Samples were analysed by IHC using anti-BRD4 antibody (Bethyl, MD, USA) (1:2000) using Dako REAL EnVision-HPR, Rabbit-Mouse kit (Dako, DK). Sections were counterstained with haematoxylin (Sigma-Aldrich Inc.). Slides were dehydrated and mounted using DPX (Sigma-Aldrich Inc.). For metastasis, paraffin sections of liver, lungs and kidney were stained with hematoxylin and eosin as described (Bhat et al, 2019). Staining intensity was assessed using a scale ranging from 0 (no staining) to 3 (strong staining) (Appendix Figs. S1 and S2D).

Mouse xenograft and metastasis models

Animal procedures were approved by Institutional Animal Care and Use Committee under protocol number R20-1589. Six-week-old C.Cg/AnNTac-Foxn1nuNE9 female BALB/c nude mice (InVivos, Singapore) were injected subcutaneously in the right flank with ten million (1×10^7) of shScr, shBRD4-L or shBRD4-S RD cells ($n = 10$/group). Tumour onset and growth were monitored and body weight was taken every alternate day. Tumour volume was calculated using the formula $V = (L \times W \times W)/2$, where V is tumour volume; W is tumour width; and L is tumour length. Once tumours in the control group reached a size of 1.5 cm in diameter, mice were sacrificed and the resected tumours were used to prepare lysates for Western blot analysis.

To analyse metastasis, shScr, shBRD4-L or shBRD4-S RD cells (1 million cells/mouse) were injected in NOD/SCID mice ($n = 10$/group) by tail vein injections. Body weights were taken every alternate day. The mice were sacrificed eight weeks after the injections. Resected tumours from the organs were used to prepare tumour lysates for Western blot analysis and the kidneys, lungs and liver were fixed in 4% PFA and processed for hematoxylin and eosin staining.

Statistical analysis

Biological assays are presented as mean ± standard error of the mean (SEM). For statistical analysis, two-tailed unpaired Student's t test for two-group comparison and one-way ANOVA with Tukey or Dunnett for multiple-group comparison using GraphPad Prism 9 (GraphPad software). P values < 0.05 were considered significant. Significance in all figures is indicated as follows: $^*p < 0.01$, $^{**}p < 0.05$, $^{***}p < 0.001$, $^{****}p < 0.0001$ and n.s. is no significance. Each experiment was performed at least thrice as independent biological replicates. Each independent experiment had three technical replicates, unless stated otherwise. All technical replicates were plotted on the scatter plots.

Data availability

The RNA-Seq data has been deposited in GEO under the accession number GSE215393.

Expanded view data, supplementary information, appendices are available for this paper at https://doi.org/10.1038/s44319-023-00033-1.

Peer review information

A peer review file is available at https://doi.org/10.1038/s44319-023-00033-1

References

Alsarraj J, Faraji F, Geiger TR, Mattaini KR, Williams M, Wu J, Ha N-H, Merlino T, Walker RC, Bosley AD et al (2013) BRD4 short isoform interacts with RRP1B, SIPA1 and components of the LINC complex at the inner face of the nuclear membrane. PLoS ONE 8:e80746

Alsarraj J, Walker RC, Webster JD, Geiger TR, Crawford NPS, Simpson RM, Ozato K, Hunter KW (2011) Deletion of the proline-rich region of the murine metastasis susceptibility gene Brd4 promotes epithelial-to-mesenchymal transition- and stem cell-like conversion. Cancer Res 71:3121–3131

Andrieu GP, Denis GV (2018) BET proteins exhibit transcriptional and functional opposition in the epithelial-to-mesenchymal transition. Mol Cancer Res 16:580–586

Asangani IA, Dommeti VL, Wang X, Malik R, Cieslik M, Yang R, Escara-Wilke J, Wilder-Romans K, Dhanireddy S, Engelke C et al (2014) Therapeutic targeting of BET bromodomain proteins in castration-resistant prostate cancer. Nature 510:278–282

Bhat AV, Palanichamy Kala M, Rao VK, Pignata L, Lim HJ, Suriyamurthy S, Chang KT, Lee VK, Guccione E, Taneja R (2019) Epigenetic regulation of the PTEN-AKT-RAC1 axis by G9a is critical for tumor growth in alveolar rhabdomyosarcoma. Cancer Res 79:2232–2243

Bid HK, Phelps DA, Xaio L, Guttridge DC, Lin J, London C, Baker LH, Mo X, Houghton PJ (2016) The bromodomain BET inhibitor JQ1 suppresses tumor angiogenesis in models of childhood sarcoma. Mol Cancer Ther 15:1018–1028

Brabletz S, Schuhwerk H, Brabletz T, Stemmler MP (2021) Dynamic EMT: a multi-tool for tumor progression. EMBO J 40:e108647

Chapuy B, McKeown MR, Lin CY, Monti S, Roemer MGM, Qi J, Rahl PB, Sun HH, Yeda KT, Doench JG et al (2013) Discovery and characterization of super-enhancer-associated dependencies in diffuse large B cell lymphoma. Cancer Cell 24:777–790

Cheng Z, Gong Y, Ma Y, Lu K, Lu X, Pierce LA, Thompson RC, Muller S, Knapp S, Wang J (2013) Inhibition of BET bromodomain targets genetically diverse glioblastoma. Clinical Cancer Research 19:1748–1759

Chiang C-M (2009) Brd4 engagement from chromatin targeting to transcriptional regulation: selective contact with acetylated histone H3 and H4. F1000 Biol Rep 1:98

Crawford NPS, Alsarraj J, Lukes L, Walker RC, Officewala JS, Yang HH, Lee MP, Ozato K, Hunter KW (2008) Bromodomain 4 activation predicts breast cancer survival. Proc Natl Acad Sci USA 105:6380–6385

Delmore JE, Issa GC, Lemieux ME, Rahl PB, Shi J, Jacobs HM, Kastritis E, Gilpatrick T, Paranal RM, Qi J et al (2011) BET bromodomain inhibition as a therapeutic strategy to target c-Myc. Cell 146:904–917

Devaiah BN, Lewis BA, Cherman N, Hewitt MC, Albrecht BK, Robey PG, Ozato K, Sims RJ, Singer DS (2012) BRD4 is an atypical kinase that phosphorylates serine2 of the RNA polymerase II carboxy-terminal domain. Proc Natl Acad Sci USA 109:6927–6932

Dobin A, Davis CA, Schlesinger F, Drenkow J, Zaleski C, Jha S, Batut P, Chaisson M, Gingeras TR (2013) STAR: ultrafast universal RNA-seq aligner. Bioinformatics 29:15–21

Donati B, Lorenzini E, Ciarrocchi A (2018) BRD4 and cancer: going beyond transcriptional regulation. Mol Cancer 17:164

Fernandez P, Scaffidi P, Markert E, Lee J-H, Rane S, Misteli T (2014) Transformation resistance in a premature aging disorder identifies a tumor-protective function of BRD4. Cell Rep 9:248–260

Filippakopoulos P, Knapp S (2014) Targeting bromodomains: epigenetic readers of lysine acetylation. Nat Rev Drug Discov 13:337–356

Gharibi A, La Kim S, Molnar J, Brambilla D, Adamian Y, Hoover M, Hong J, Lin J, Wolfenden L, Kelber JA (2017) ITGA1 is a pre-malignant biomarker that promotes therapy resistance and metastatic potential in pancreatic cancer. Sci Rep 7:10060

Gryder BE, Yohe ME, Chou H-C, Zhang X, Marques J, Wachtel M, Schaefer B, Sen N, Song Y, Gualtieri A et al (2017) PAX3-FOXO1 establishes myogenic super enhancers and confers BET bromodomain vulnerability. Cancer Discov 7:884–899

Hamidi H, Ivaska J (2018) Every step of the way: integrins in cancer progression and metastasis. Nat Rev Cancer 18:533–548

Han X, Yu D, Gu R, Jia Y, Wang Q, Jaganathan A, Yang X, Yu M, Babault N, Zhao C et al (2020) Roles of the BRD4 short isoform in phase separation and active gene transcription. Nat Struct Mol Biol 27:333–341

Hawkins DS, Spunt SL, Skapek SX, COG Soft Tissue Sarcoma Committee (2013) Children's Oncology Group's 2013 blueprint for research: Soft tissue sarcomas. Pediatr Blood Cancer 60:1001–1008

Jiao Y, Li Y, Liu S, Chen Q, Liu Y (2019) ITGA3 serves as a diagnostic and prognostic biomarker for pancreatic cancer. Onco Targets Ther 12:4141–4152

Kurimchak AM, Shelton C, Duncan KE, Johnson KJ, Brown J, O'Brien S, Gabbasov R, Fink LS, Li Y, Lounsbury N et al (2016) Resistance to BET bromodomain inhibitors is mediated by kinome reprogramming in ovarian cancer. Cell Rep 16:1273–1286

Lenhart R, Kirov S, Desilva H, Cao J, Lei M, Johnston K, Peterson R, Schweizer L, Purandare A, Ross-Macdonald P et al (2015) Sensitivity of small cell lung cancer to BET inhibition is mediated by regulation of ASCL1 gene expression. Mol Cancer Ther 14:2167–2174

Li S, Zhang N, Liu S, Zhang H, Liu J, Qi Y, Zhang Q, Li X (2022) ITGA5 is a novel oncogenic biomarker and correlates with tumor immune microenvironment in gliomas. Front Oncol 12:844144

Ling BMT, Bharathy N, Chung T-K, Kok WK, Li S, Tan YH, Rao VK, Gopinadhan S, Sartorelli V, Walsh MJ et al (2012) Lysine methyltransferase G9a methylates the transcription factor MyoD and regulates skeletal muscle differentiation. Proc Natl Acad Sci USA 109:841–846

Loh WE, Scrable HJ, Livanos E, Arboleda MJ, Cavenee WK, Oshimura M, Weissman BE (1992) Human chromosome 11 contains two different growth suppressor genes for embryonal rhabdomyosarcoma. Proc Natl Acad Sci USA 89:1755–1759

Marchesi I, Fais M, Fiorentino FP, Bordoni V, Sanna L, Zoroddu S, Bagella L (2022) Bromodomain inhibitor JQ1 provides novel insights and perspectives in rhabdomyosarcoma treatment. Int J Mol Sci 23:3581

Masià A, Almazán-Moga A, Velasco P, Reventós J, Torán N, Sánchez de Toledo J, Roma J, Gallego S (2012) Notch-mediated induction of N-cadherin and α9-integrin confers higher invasive phenotype on rhabdomyosarcoma cells. Br J Cancer 107:1374–1383

Megiorni F (2020) Epigenetics in rhabdomyosarcoma: cues to new biomarkers and targeted therapies. EBioMedicine 52:102673

Pal A, Leung JY, Ang GCK, Rao VK, Pignata L, Lim HJ, Hebrard M, Chang KT, Lee VK, Guccione E et al (2020) EHMT2 epigenetically suppresses Wnt signaling and is a potential target in embryonal rhabdomyosarcoma. eLife 9:e57683

Parham DM, Barr FG (2013) Classification of rhabdomyosarcoma and its molecular basis. Adv Anat Pathol 20:387–397

Proserpio V, Fittipaldi R, Ryall JG, Sartorelli V, Caretti G (2013) The methyltransferase SMYD3 mediates the recruitment of transcriptional cofactors at the myostatin and c-Met genes and regulates skeletal muscle atrophy. Genes Dev 27:1299–1312

Pulkka O-P, Mpindi J-P, Tynninen O, Nilsson B, Kallioniemi O, Sihto H, Joensuu H (2018) Clinical relevance of integrin alpha 4 in gastrointestinal stromal tumours. J Cell Mol Med 22:2220–2230

Ricaud S, Vernus B, Duclos M, Bernardi H, Ritvos O, Carnac G, Bonnieu A (2003) Inhibition of autocrine secretion of myostatin enhances terminal differentiation in human rhabdomyosarcoma cells. Oncogene 22:8221–8232

Shern JF, Chen L, Chmielecki J, Wei JS, Patidar R, Rosenberg M, Ambrogio L, Auclair D, Wang J, Song YK et al (2014) Comprehensive genomic analysis of rhabdomyosarcoma reveals a landscape of alterations affecting a common genetic axis in fusion-positive and fusion-negative tumors. Cancer Discov 4:216–231

Shu S, Lin CY, He HH, Witwicki RM, Tabassum DP, Roberts JM, Janiszewska M, Huh SJ, Liang Y, Ryan J et al (2016) Response and resistance to BET bromodomain inhibitors in triple-negative breast cancer. Nature 529:413–417

Skapek SX, Ferrari A, Gupta A, Lupo PJ, Butler E, Shipley J, Barr FG, Hawkins DS (2019) Rhabdomyosarcoma. Nat Rev Dis Primers 5:1

Slavish PJ, Chi L, Yun M-K, Tsurkan L, Martinez NE, Jonchere B, Chai SC, Connelly M, Waddell MB, Das S et al (2020) Bromodomain-selective BET inhibitors are potent antitumor agents against MYC-driven pediatric cancer. Cancer Res 80:3507–3518

Srivastava RK, Guroji P, Jin L, Mukhtar MS, Athar M (2022) Combined inhibition of BET bromodomain and mTORC1/2 provides therapeutic advantage for rhabdomyosarcoma by switching cell death mechanism. Mol Carcinog 61:737–751

Stathis A, Bertoni F (2018) BET proteins as targets for anticancer treatment. Cancer Discov 8:24–36

Wang L, Xu M, Kao C-Y, Tsai SY, Tsai M-J (2020) Small molecule JQ1 promotes prostate cancer invasion via BET-independent inactivation of FOXA1. J Clin Invest 130:1782–1792

Williamson D, Missiaglia E, de Reyniès A, Pierron G, Thuille B, Palenzuela G, Thway K, Orbach D, Laé M, Fréneaux P et al (2010) Fusion gene-negative alveolar rhabdomyosarcoma is clinically and molecularly indistinguishable from embryonal rhabdomyosarcoma. J Clin Oncol 28:2151–2158

Wolfer A, Ramaswamy S (2011) MYC and Metastasis. Cancer Res 71:2034–2037
Wu S-Y, Chiang C-M (2007) The double bromodomain-containing chromatin adaptor Brd4 and transcriptional regulation. J Biol Chem 282:13141–13145
Wu S-Y, Lee C-F, Lai H-T, Yu C-T, Lee J-E, Zuo H, Tsai SY, Tsai M-J, Ge K, Wan Y et al (2020) Opposing functions of BRD4 isoforms in breast cancer. Molecular Cell 78:1114–1132.e10
Xia SJ, Pressey JG, Barr FG (2002) Molecular pathogenesis of rhabdomyosarcoma. Cancer Biol Ther 1:97–104
Zeng L, Zhou MM (2002) Bromodomain: an acetyl-lysine binding domain. FEBS Lett 513:124–128
Zhang Y, Xu B, Shi J, Li J, Lu X, Xu L, Yang H, Hamad N, Wang C, Napier D et al (2020) BRD4 modulates vulnerability of triple-negative breast cancer to targeting of integrin-dependent signaling pathways. Cell Oncol 43:1049–1066
Zuber J, Shi J, Wang E, Rappaport AR, Herrmann H, Sison EA, Magoon D, Qi J, Blatt K, Wunderlich M et al (2011) RNAi screen identifies Brd4 as a therapeutic target in acute myeloid leukaemia. Nature 478:524–528

Acknowledgements

We thank Peter Houghton and Rosella Rota for the ERMS cell lines. This work was supported by a Ministry of Education MOE2019-T2-1-024 grant and a National Medical Research Council grant MOH-001389-01 to RT. C-MC's research is supported by US NIH grant 1RO1CA251698-01 and CPRIT grant RP180349. JYL was supported by a PhD scholarship from the Agency for Science, Technology and Research (A*STAR). We thank Dr. Nandini Karthik and Dr. Hsin Yao Chiu for their comments on the manuscript.

Author contributions

Dipanwita Das: Conceptualization; Formal analysis; Validation; Investigation; Methodology; Writing—original draft; Writing—review and editing. **Jia Yu Leung**: Formal analysis; Investigation. **Shivaranjani Balamurugan**: Validation; Investigation; Visualization. **Vinay Tergaonkar**: Supervision. **Amos Hong Pheng Loh**: Data curation; Supervision; Validation; Visualization. **Cheng-Ming Chiang**: Resources; Methodology; Writing—original draft. **Reshma Taneja**: Conceptualization; Supervision; Funding acquisition; Writing—original draft; Writing—review and editing.

Disclosure and competing interests statement

The authors declare no competing interests.

Expanded View Figures

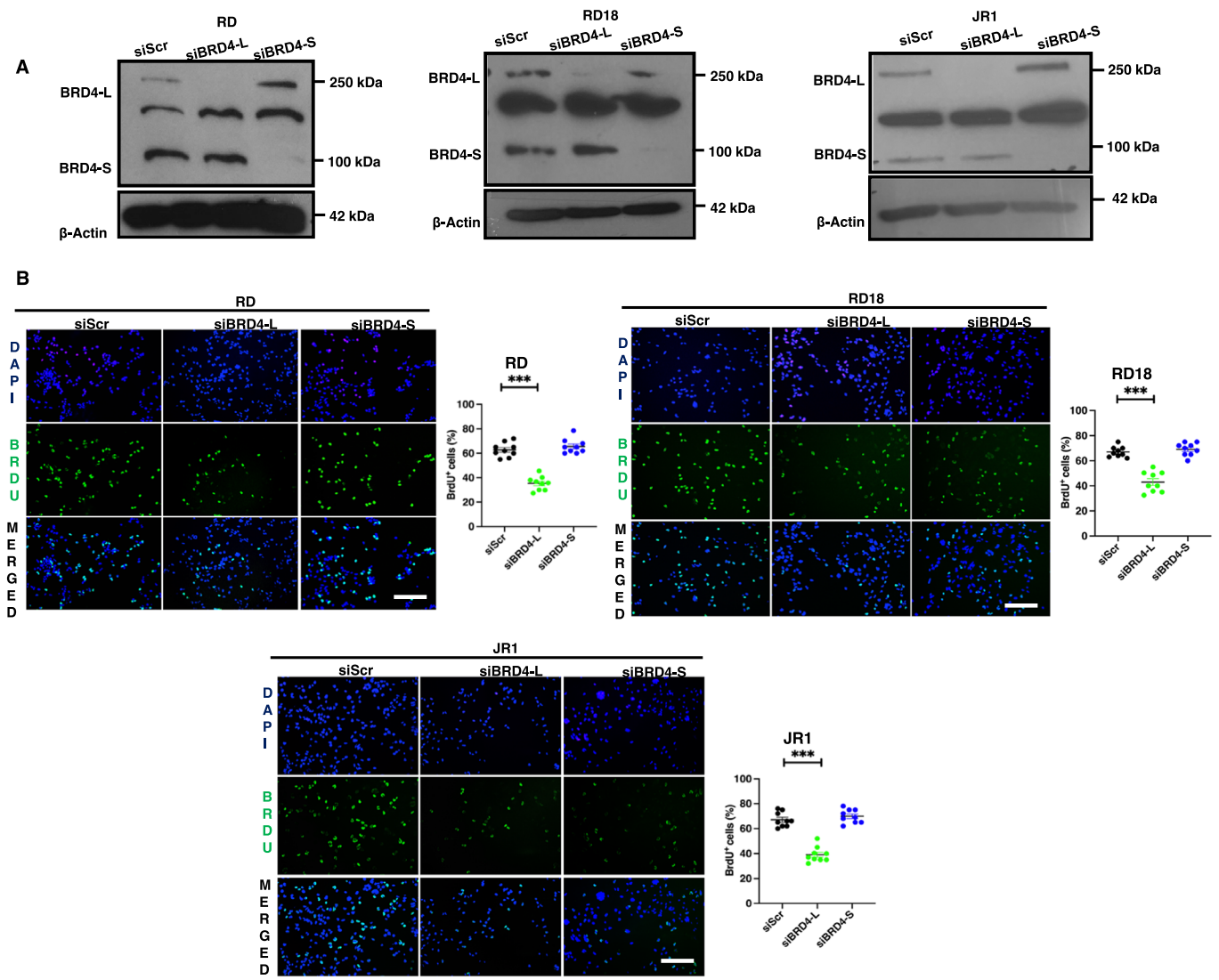

Figure EV1. BRD4-L knockdown represses proliferation.

(**A**) Western blot analysis showing transient BRD4 knockdown efficiency in siBRD4-L and siBRD4-S RD, RD18 and JR1 cells as indicated. β-Actin was used as the loading control. Images are representative of at least three biological replicates. (**B**) Proliferation was analysed by BrdU assay in control (siScr), siBRD4-L and siBRD4-S RD, RD18 and JR1 cells as indicated. Images are representative of at least three biological replicates. Scale bar: 100 µm. Scatter plot showing the percentage of $BrdU^+$ cells in siScr, siBRD4-L and siBRD4-S cells. Values correspond to the average ± SEM ($n = 3$ biological replicates with 3 technical replicates shown). Two-tailed non-parametric unpaired t test was performed for statistical analysis. ***$p \leq 0.001$.

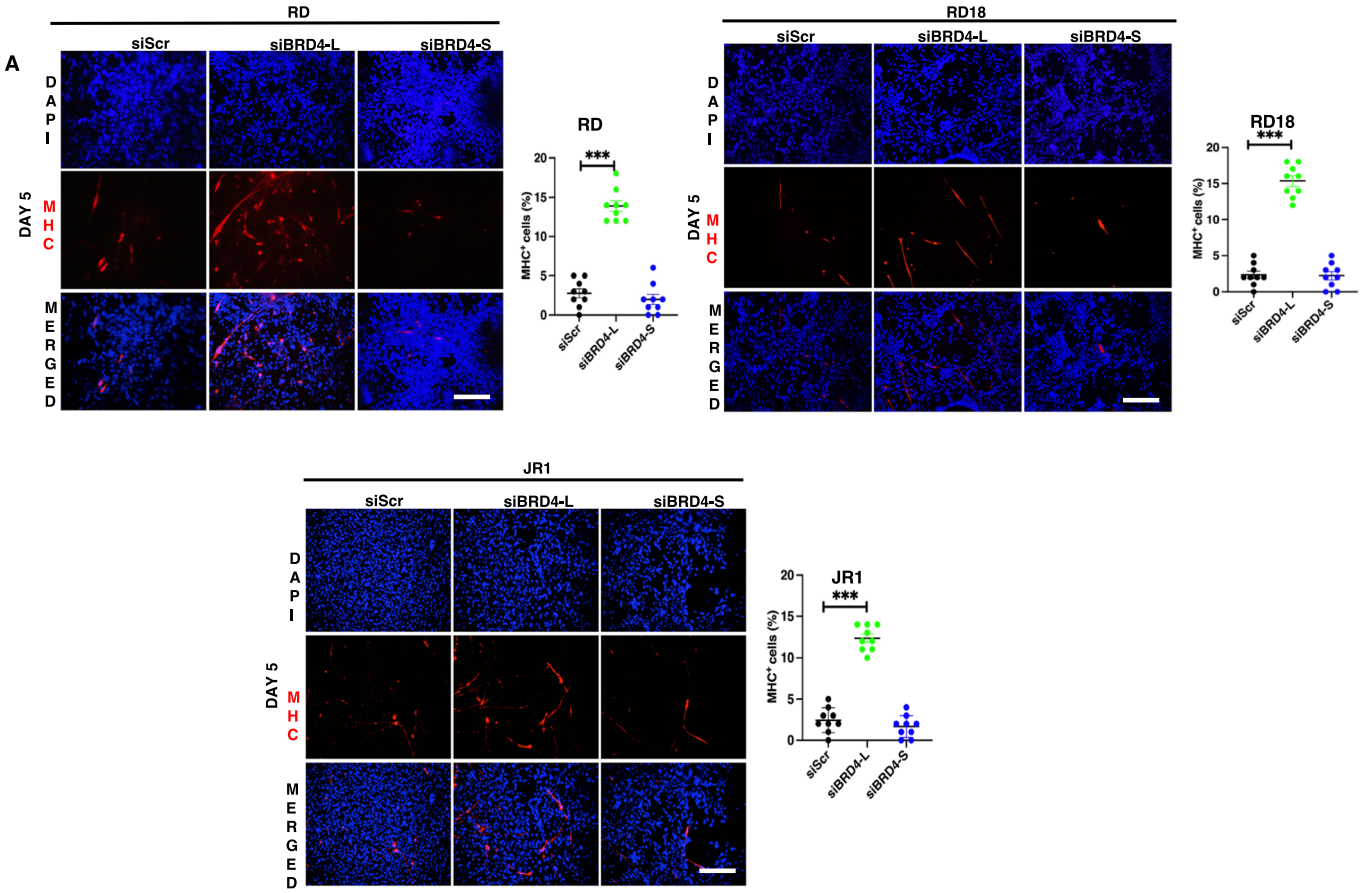

Figure EV2. BRD4-L knockdown enhances differentiation.

(**A**) Differentiation was analysed by immunofluorescence in siScr, siBRD4-L and siBRD4-S in RD, RD18 and JR1 cells as indicated. Forty-eight hours post-transfection, cells were cultured in differentiation media for 5 days and MHC$^+$ cells were analysed using anti-MHC antibody. Images are representative of at least three biological replicates. Nuclei were stained with DAPI (blue). Scale bar: 100 µm. Scatter plots indicating the percentage of MHC$^+$ cells in siScr, siBRD4-L and siBRD4-S cells. Values correspond to the average ± SEM ($n = 3$ biological replicates with 3 technical replicates shown). Two-tailed non-parametric unpaired t test was performed for statistical analysis. ***$p \leq 0.001$.

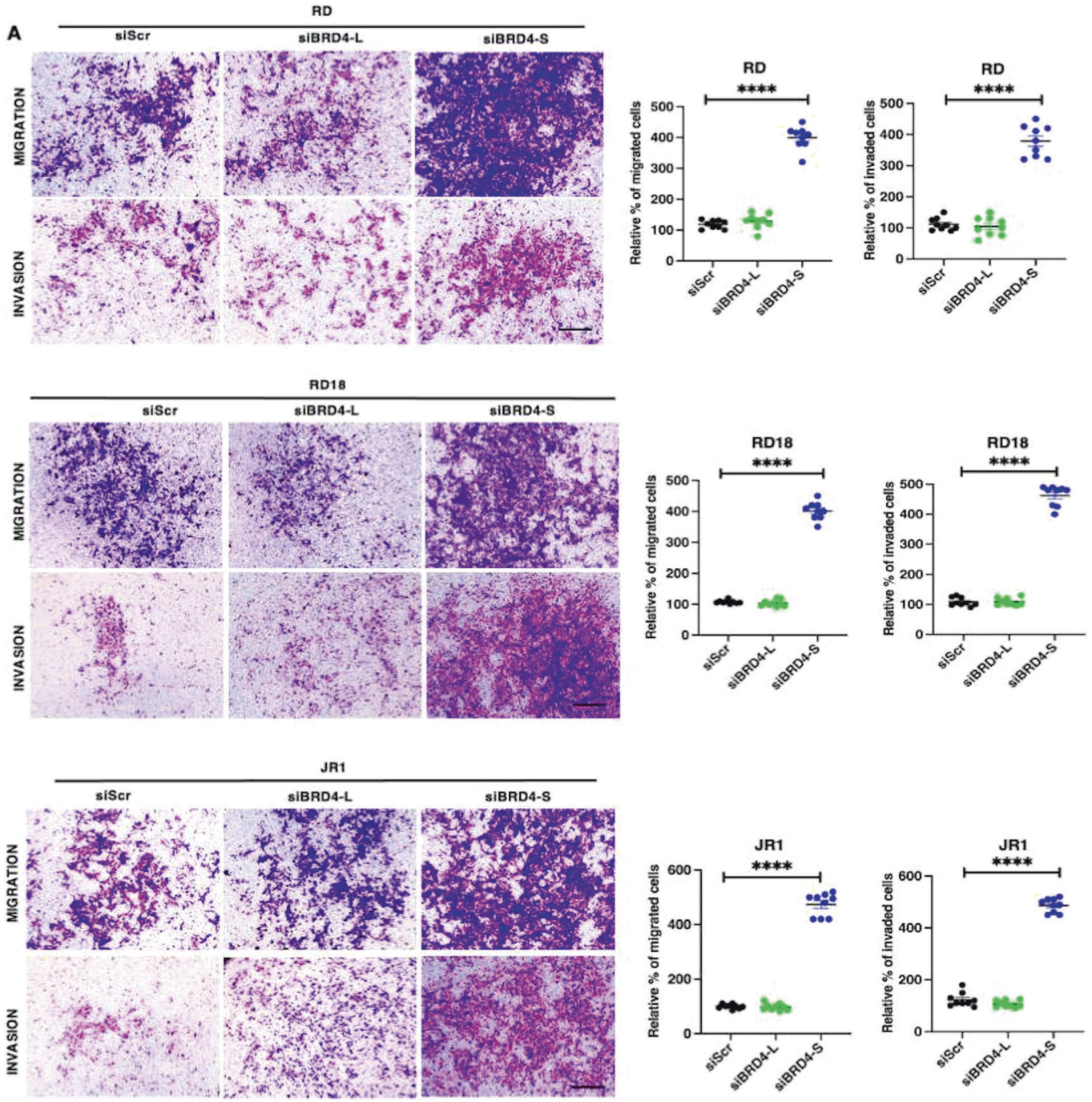

Figure EV3. BRD4-S knockdown increases cellular migration and invasion.

(**A**) Migration and invasion was analysed by Transwell assays in siScr, siBRD4-L and siBRD4-S RD, RD18 and JR1 cells as indicated. The inserts were stained with crystal violet. Images are representative of at least three biological replicates. Scale bar: 100 µm. Scatter plots indicating the percentage of migration and invasion is shown. Values correspond to the average ± SEM. Values correspond to the average ± SEM ($n = 3$ biological replicates with 3 technical replicates shown). Two-tailed non-parametric unpaired t test was performed for statistical analysis. ****$p \leq 0.0001$.

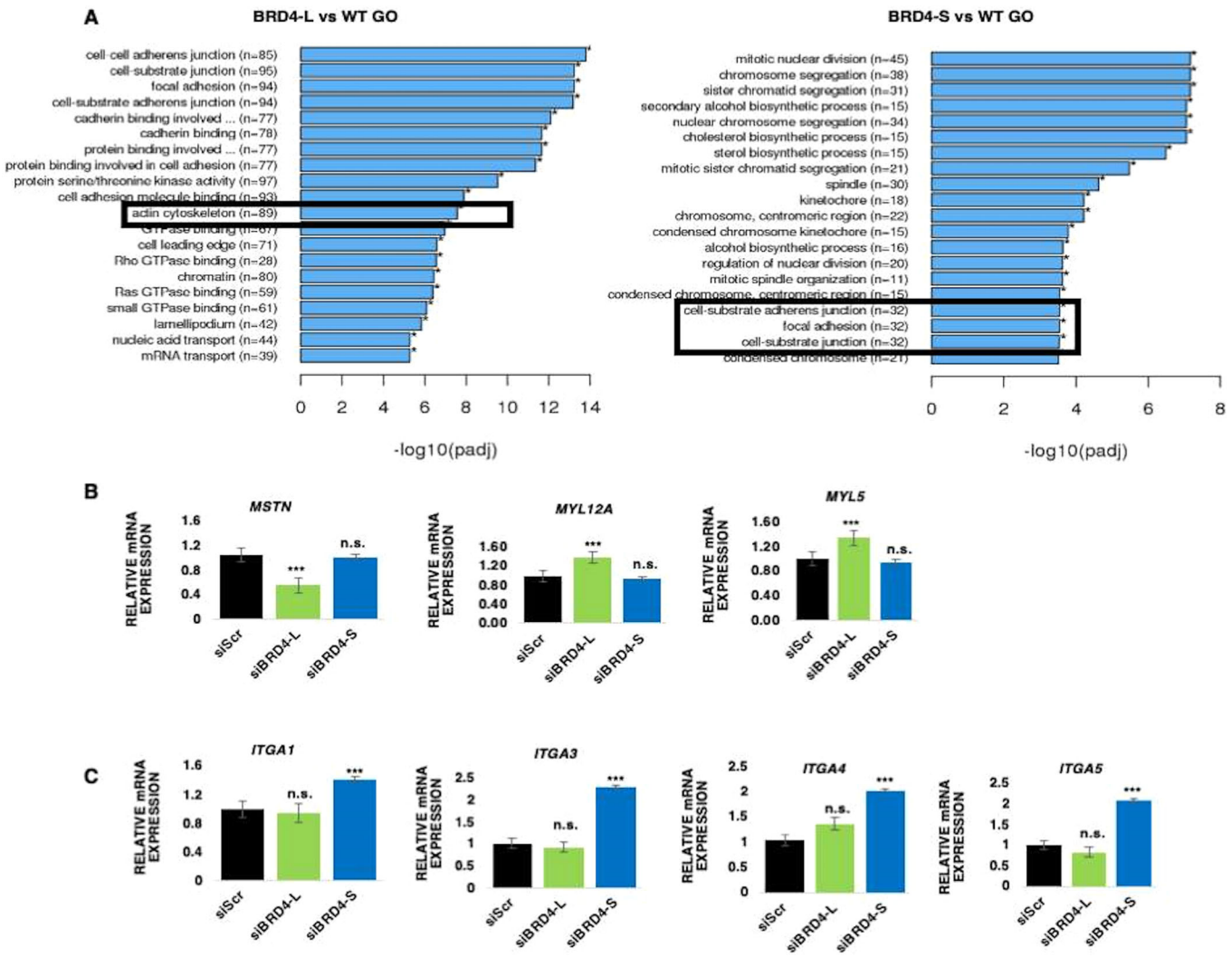

Figure EV4. Validation of BRD4-L and BRD4-S targets.

(**A**) GO enrichment histogram showing significantly enriched biological processes upon BRD4-L and BRD4-S knockdown based on the number of differentially expressed genes. (**B**) RT-qPCR analysis of *MSTN*, *MYL12A* and *MYL5* mRNA in siScr, siBRD4-L and siBRD4-S cells. The values correspond to average ± SEM ($n = 4$ biological replicates). n.s. = not significant, ***$p \leq 0.001$, n.s. not significant. (**C**) RT-qPCR analysis of the integrin (*ITGA1, ITGA3, ITGA4* and *ITGA5*) mRNA in siScr, siBRD4-L and siBRD4-S cells. The values correspond to average ± SEM ($n = 4$ biological replicates). Two-tailed non-parametric unpaired t test was performed for statistical analysis. n.s. not significant, ***$p \leq 0.001$, n.s. not significant.

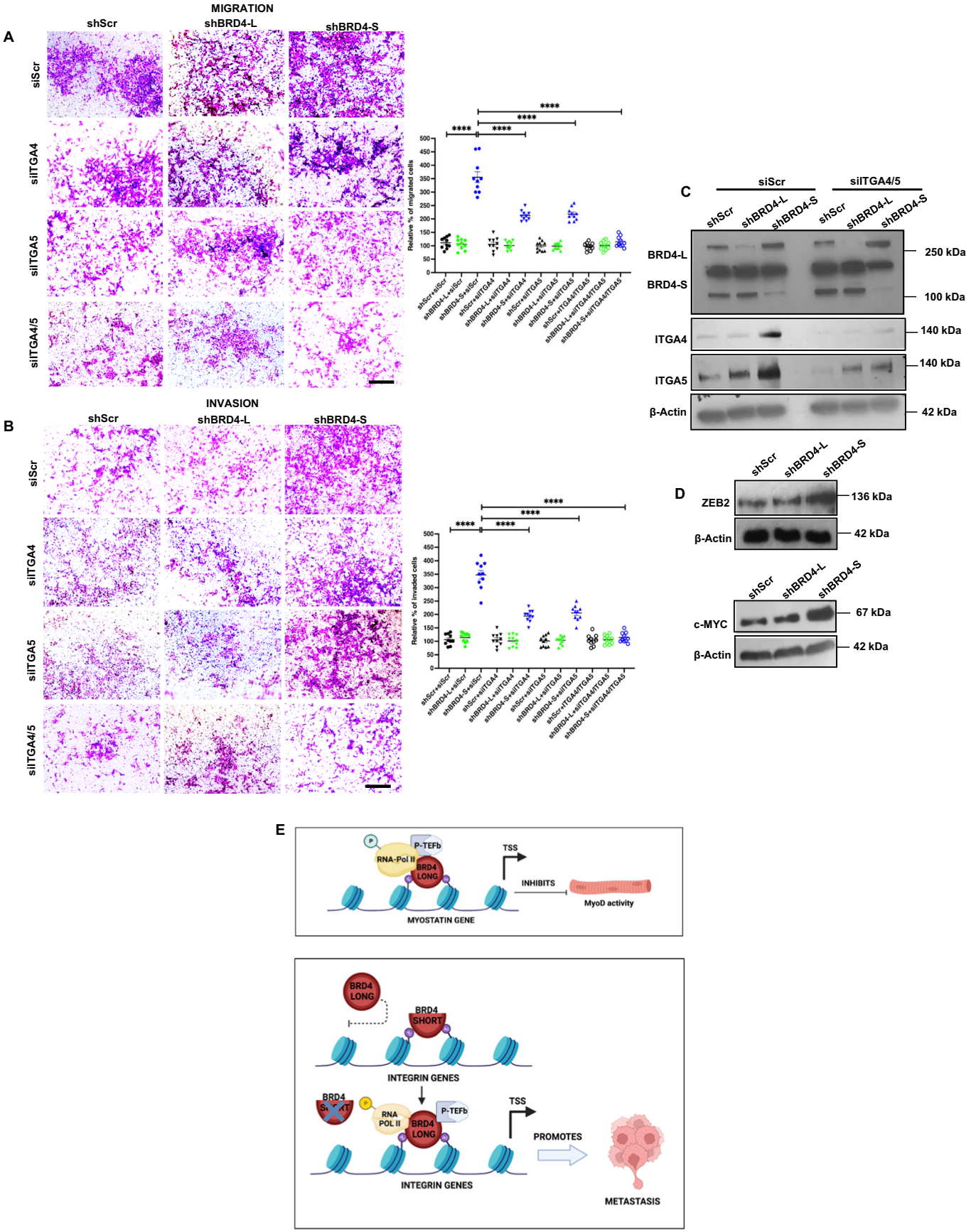
A
MIGRATION
shScr
shBRD4-L
shBRD4-S
siScr
siITGA4
siITGA5
siITGA4/5
Relative % of migrated cells
B
INVASION
Relative % of invaded cells
C
siScr
siITGA4/5
BRD4-L
BRD4-S
ITGA4
ITGA5
β-Actin
250 kDa
100 kDa
140 kDa
140 kDa
42 kDa
D
ZEB2
136 kDa
42 kDa
c-MYC
67 kDa
42 kDa
E
P-TEFb
RNA-Pol II
BRD4 LONG
TSS
INHIBITS
MyoD activity
MYOSTATIN GENE
BRD4 SHORT
INTEGRIN GENES
PROMOTES
METASTASIS

Figure EV5. ITGA4/5 knockdown rescues migration and invasion in shBRD4-S cells.

(**A**,**B**) Migration and invasion was analysed by Transwell assays in shScr, shBRD4-L and shBRD4-S by transfecting them with siScr, siITGA4, siITGA5 or siITGA4 and 5. The inserts were stained with crystal violet. Images are representative of at least three biological replicates. Scale bar: 100 µm. Scatter plots indicating the percentage of migration and invasion is shown. Error bars correspond to the average ± SEM ($n = 5$ biological replicates with 2 technical replicates shown). Two-tailed non-parametric unpaired t test was performed for statistical analysis. ***$p \leq 0.001$, ****$p \leq 0.0001$. (**C**) Western blot analysis showing transient ITGA4 and ITGA5 knockdown efficiency in shScr, shBRD4-L and shBRD4-S cells as indicated. β-Actin was used as the loading control. Images are representative of at least three biological replicates. (**D**) Western blot analysis showing ZEB2 and c-MYC expression in shScr, shBRD4-L and shBRD4-S cells as indicated. β-Actin was used as the loading control. Images are representative of at least two biological replicates. (**E**) Graphical model summarizing the function of the BRD4 isoforms in ERMS. Source data are available online for this figure.

